Diyala Journal of Engineering Sciences

Journal homepage: https://djes.info/index.php/djes

ISSN: 1999-8716 (Print); 2616-6909 (Online)

Machine Learning-Based High-Isolation Dual-Band MIMO Antenna with Gain Prediction for 5G Networks at 28/38 GHz

Md Mahabub Alam[1*], Md. Ashraful Haque[2], Md Ershadul Haque[3], Md. Suaibur Rahman[4]

[1]Faculty of Electrical Engineering Technology, University of Quebec at Trois-Rivières, Trois-Rivières, Québec G8Z 4M3, Canada
[2] Department of Electrical and Electronic Engineering, University of Liberal Arts Bangladesh (ULAB), Dhaka 1207, Bangladesh
[3]School of Computing Mathematics and Engineering, Charles Sturt University, Bathurst, NSW, 2795, Australia.
[4]Department of Electrical Electronics Engineering Technology, Islamic University of Technology, Gazipur-1704, Dhaka, Bangladesh

ARTICLE INFO

Article history:
Received: 9/05/2026.
Revised: 12/08/2026,
Accepted: 13/08/2026,
Available online: 15/09/2026.

Keywords:
MIMO
28 GHz and 38 GHz
Machine Learning
Regression Model
5G

ABSTRACT

This paper proposes an ML-driven compact dual-band four-port MIMO antenna for next-generation 5G mm-wave communications at 28/38 GHz. The challenge of integrating ML-based gain prediction with a high-isolation four-element MIMO architecture is discussed. The antenna is designed on a Rogers RT/duroid 6002 substrate with a small footprint of 15.82 × 15.82 mm² (1.48λ₀ × 1.48λ₀) and is systematically evolved from a single element to 2-port and 4-port MIMO configurations with the maximum gains of 8.5 dBi and 7.25 dBi with the radiation efficiencies of 95% and 96% at 28 GHz and 38 GHz, respectively. The 4-port MIMO system shows excellent isolation over 30 dB, envelope correlation coefficient below 0.001, diversity gain over 0.95, and channel capacity loss of only 0.01 bps/Hz at 28 GHz, which confirms the excellent spatial diversity and spectral efficiency for 5G deployment. To accelerate the design cycle, a comprehensive ML framework was developed using six advanced regression algorithms, with inputs including key geometrical parameters like slot dimensions, impedance transformer geometry and feed line specifications. Among the models evaluated, the Extra Trees Regressor model achieved the best predictive performance with over 98% accuracy in the estimation of the bandwidth at 38 GHz and approximately 94% accuracy in the prediction of the gain at 28 GHz. This provides a scalable design paradigm for future mm-wave MIMO antennas and enables a fast simulation-free performance prediction method. Extra Trees predictions, validated through test-set evaluation and K-fold cross-validation, confirm effectiveness of the proposed four-port MIMO antenna for 28/38-GHz 5G applications.

1. INTRODUCTION

The rapid development of fifth generation (5G) wireless communication systems has increased the need for high data rate, low latency and spectrum efficient technologies that can support emerging applications such as ultra-high-definition streaming, autonomous systems and massive Internet of Things (IoT) connectivity as shown in Figure 1 [1]. Millimetre-wave (mm-wave) frequency bands especially at 28 GHz and 38 GHz have been identified as key enablers to fulfill these requirements owing to their wide available bandwidth [2]. However, the use of these bands introduces challenging design issues, such as high propagation losses, increased mutual coupling in small antenna arrays, and the need for efficient spatial diversity techniques.

One of the most powerful enablers of high-capacity 5G communication is multiple-input multiple-output (MIMO) antenna technology, which employs spatial multiplexing and diversity techniques to dramatically improve channel capacity and link reliability without additional spectral resources [3]. One of the main design challenges in mm-wave MIMO systems is to achieve high inter-element isolation, as the mutual coupling between the antenna elements in close proximity directly degrades the radiation performance, increases the envelope correlation and decreases the effective diversity gain of the system [4]. Therefore, the design of compact and dual-band MIMO antennas with high

*Corresponding author's E-mail: Md.Mahabub.Alam@uqtr.ca | ORCID: 0009-0005-5036-4608
DOI: 10.24237/djes.2026.19301

gain, high isolation and excellent diversity performance simultaneously at 28/38 GHz is of significant research interest and practical urgency.

Much research has been carried out for mm-wave antenna design for 5G applications. Slot-based and patch antenna configurations on low-loss substrates have been widely explored, with various decoupling mechanisms, including defected ground structures (DGS), neutralization lines, parasitic elements, and electromagnetic bandgap (EBG) structures, employed to suppress mutual coupling [5–7]. While most reported designs achieve isolation of around 20–35 dB, the challenge of achieving more than 50 dB of isolation in a compact four-port MIMO form factor is still a challenging task, with only a few works demonstrating this, especially in dual operating bands concurrently [8]. Secondly, a detailed assessment of MIMO diversity metrics, such as an envelope correlation coefficient (ECC), diversity gain (DG), and channel capacity loss (CCL) is required to evaluate the practical applicability of these antenna systems in dense 5G deployment scenarios.

Figure 1. Applications of 5G mm-wave (28/38 GHz) Spectrum [2].

To meet this combined isolation, gain and diversity goals usually requires a large iterative optimization process in a large interdependent geometric parameter space, making the design process itself a major effort. The challenge of accelerating the antenna design cycle is equally important. Full-wave electromagnetic (EM) simulations are very accurate but computationally intensive and time consuming especially for complex multi-port MIMO structures with a large number of interdependent geometrical parameters [9]. Achieving stringent 5G performance targets, such as resonance frequency, impedance bandwidth, gain and isolation, requires an iterative optimization process that may take weeks of simulation time and represents a key bottleneck in the development of next-generation wireless hardware. This has led to increasing interest in machine learning (ML)-aided performance prediction as a complementary tool to the antenna design process, with the promise of a fast, data-driven estimate of performance parameters without the overhead of repeated full-wave simulation once a candidate design is established [10]. Such ML frameworks are important to note to be downstream of the electromagnetic design process: the physical optimization of the antenna geometry is not replaced or driven by the ML framework, but rather the mapping between geometric parameters and simulated performance outcomes is learned to accelerate subsequent design evaluation. The potential of ML as a predictive tool in antenna engineering has been increasingly demonstrated [11]. Using geometrical and material parameters as inputs, regression-based models, neural networks, and ensemble learning algorithms have predicted antenna resonance frequencies, gain profiles, S-parameters, and bandwidth with high accuracy [12–14]. In particular, among the various ML algorithms, k-nearest neighbor (KNN) regression and ensemble methods such as Extra Trees Regressors have shown promising results in the task of antenna parameter prediction, exhibiting good generalization, robustness to overfitting, and high accuracy for different antenna geometries [15]. However, the implementation of a complete ML prediction framework along with a high-isolation dual-band MIMO antenna targeting 28/38 GHz 5G applications has not been well addressed in the existing literature. To overcome these problems, in this paper, a compact dual-band four-port MIMO antenna with Rogers RT/duroid 6002 substrate for 5G mm-wave applications at 28 GHz and 38 GHz is presented by using ML. The main contributions of this work are summarized as follows:

i. A compact dual-band four-port MIMO antenna in a footprint of $1.48\lambda_0 \times 1.48\lambda_0$ mm² achieving peak gains of 8.5 dBi and 7.25 dBi with radiation efficiencies of 95% and 96% at 28 GHz and 38 GHz respectively.

ii. Over 30 dB of superior 4-port MIMO isolation, ECC less than 0.001, diversity gain over 0.95 and only 0.01 bps/Hz channel capacity loss at 28 GHz, achieving best-in-class diversity performance.

iii. We develop a comprehensive ML regression framework using six algorithms to enable simulation-free gain prediction. Extra Trees Regression achieves the best performance with 98% prediction accuracy for gain prediction and 94% prediction accuracy for bandwidth prediction.

iv. Rigorous ML model validation using K-fold cross-validation to ensure robust generalization and to establish a scalable, data-driven design paradigm for next generation mm-wave MIMO antenna engineering.

2. DESIGN METHODOLOGY

The proposed four-element slotted MIMO antenna was designed and optimized based on a systematic iterative development process as shown in Figure 2. The process begins with the design and simulation of a single crescent-shaped antenna element in CST Microwave

Studio where the key performance indicators, namely the reflection coefficient (S_{11}), gain and radiation efficiency are evaluated. If the simulated performance is not satisfactory, the input parameters are iteratively refined by a parametric sweep until all single element performance requirements are satisfied, providing the best single element antenna result. After the successful optimization of the single element, the design is gradually scaled to a two-element MIMO configuration. Then, the critical MIMO performance indicators, such as S_{11}, S_{21} (isolation), Envelope Correlation Coefficient (ECC), Diversity Gain (DG), gain and radiation efficiency are analyzed in detail. If the results are not satisfactory, mutual coupling is reduced by a suitable method, i.e., Defected Ground Structure (DGS) and inter element distance adjustment. The two-element configuration is iteratively refined until all the diversity and isolation requirements are met. After the design of the two element MIMO is completed, the architecture is extended to four element MIMO setup. An analogous set of performance evaluations, namely S_{11}, S_{21}, ECC, DG, gain and radiation efficiency is performed to ensure maximum spatial diversity and minimal mutual coupling. Coupling reduction is again achieved thru DGS and distance optimization where required. The iterative optimization process is continued until all the performance indicators reach the desired thresholds, which results in a final compact four-element MIMO antenna for 5G mm-wave applications at 28/38 GHz.

3. ANALYSIS OF FOUR ELEMENT MIMO ANTENNA

3.1 Single Antenna Design

When a high frequency signal is applied, the patch is excited and resonant electromagnetic modes are induced [16]. Radiation occurs mainly at the edges of the patch where fringing electric fields extend into air, allowing the conversion of the guided wave to free space radiation. When the patch length is designed to be a little less than half the guided wavelength (λ/2), it resonates in the fundamental transverse magnetic (TM_{10}) mode, producing a standing wave of current along its length. This resonance causes efficient edge radiation, which makes the microstrip antenna an efficient and compact radiator for modern wireless systems [17]. The width (W) and length (L) of the patch that determines its resonant behavior is calculated using Eq. (1) and (2) respectively [17].

$$W = \frac{c}{2f_r\sqrt{\frac{(\varepsilon_r+1)}{2}}} \tag{1}$$

Where c is the speed of light, f_r is the resonance frequency of the antenna, ε_r is the dielectric constant of the substrate [18].

$$L = \frac{c}{2f_r\sqrt{\varepsilon_{eff}}} - \Delta L \tag{2}$$

Here, ΔL is the length correction due to fringing effects, ε_{eff} is the effective dielectric constant

The effective dielectric constant is defined by Eq. (3).

$$\varepsilon_{eff} = \frac{\varepsilon_r+1}{2} + \frac{\varepsilon_r-1}{2}\left[1+12\left(\frac{h}{W}\right)\right]^{-1/2} \tag{3}$$

Here, h is the thickness of the substrate, W is the width of the microstrip antenna, ε_r is the dielectric constant of the substrate.

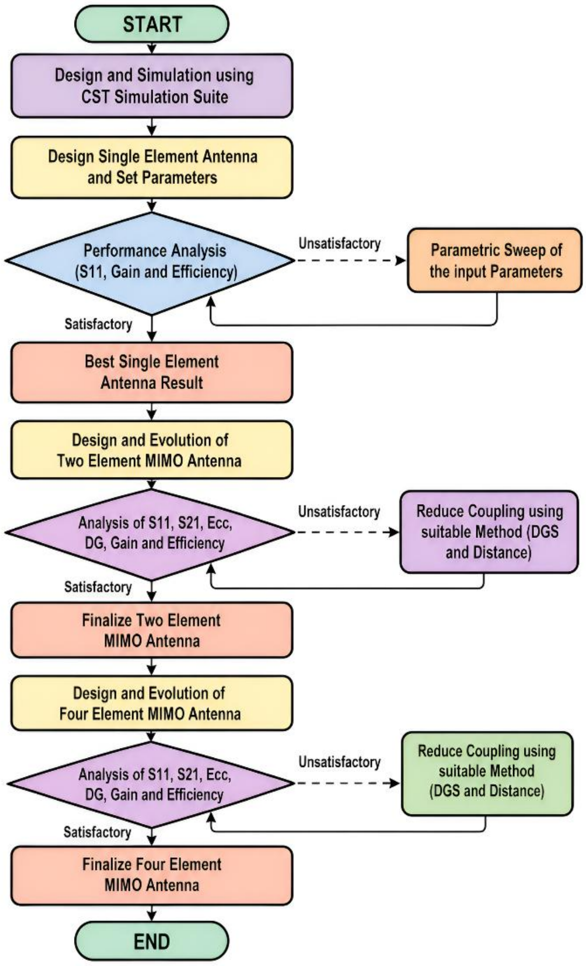

Figure 2. Flowchart of the design evolution and performance evaluation of the proposed four-element MIMO antenna.

Proper impedance matching is achieved by the inset feed technique. The feed is not at the edge of the patch where the impedance is usually high but is instead recessed inward a certain distance to a point where the impedance is better matched to the 50-ohm feed line [17]. This lowers the return loss and improves overall efficiency of power transfer. Further improvement of the impedance matching can also be obtained by using quarter wave transformer. Its length, L_T is given by Eq. (4).

$$L_T = \frac{\lambda_g}{4} \tag{4}$$

Here, λg being the guided wavelength based on the effective dielectric constant.

By using this principle, the single element antenna was fabricated on a Rogers RT/duroid 6002 substrate (ε_r=2.94, h=0.32 mm) with the best wave confinement and propagation features in a small area of 7.91 mm × 7.85 mm. It can be seen from Table 1, the ground plane

(7.91 mm × 7.2 mm) has good electromagnetic isolation effect, and the radiating patch (4.73 mm × 3.055 mm) is the main electromagnetic wave launcher. The impedance matching network comprises a quarter-wave transformer (0.7 mm x 2.4 mm) and a feedline (2.5 mm x 1.2 mm) which are properly dimensioned, to ensure an effective power transfer in the operational frequency bands. The single element contains four well-optimized sections, namely, Slot 1 (2.6 mm × 0.17 mm), Slot 2 (0.2 mm × 1.6 mm), Slot 3 (0.5 mm × 0.39 mm), and Slot 4 (0.15 mm × 0.33 mm). Each slot is designed to suppress the unwanted higher order modes and control the cut-off frequency that enables a better impedance matching dual-band operation. Figure 3 shows the design geometry of the single element antenna with its important dimensions.

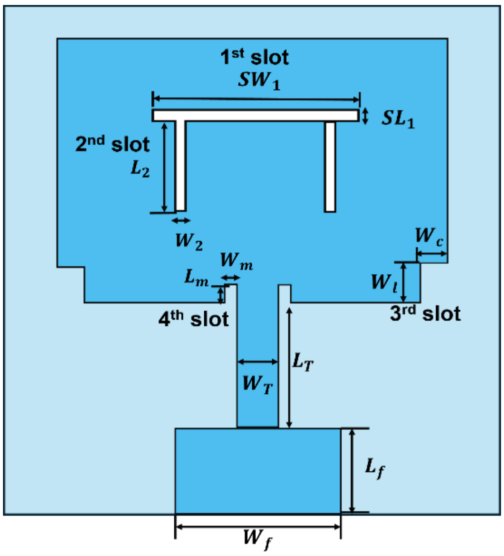

Figure 3. Single-element antenna top view configuration.

Table 1. Optimized dimensions of proposed π-slotted patch antenna

Design Parameter	Variable description	Optimized Value [mm]
W_g	Width of ground	7.91
L_g	Length of ground	7.2
W_s	Width of the substrate	7.91
L_s	Length of substrate	7.85
W	Width of the patch	4.73
L	Length of patch	3.055
h	Height of substrate	0.254
W_T	Width of transformer	0.7
L_T	Length of transformer	2.4
W_f	Width of feedline	2.5
L_f	Length of feedline	1.2
$SW_1 \times SL_1$	Dimension of slot 1	2.6 × 0.17
$W_2 \times L_2$	Dimension of slot 2	0.2 × 1.6
$W_c \times W_L$	Dimension of slot 3	0.5 × 0.39
$W_m \times L_m$	Dimension of slot 4	0.15 × 0.33

Figure 4 presents the simulated reflection coefficient (S_{11}) and realized gain of the proposed single-element antenna across the 26–40 GHz frequency range, as shown in (a) and (b), respectively. As shown in Figure 4 (a), the proposed single-element antenna exhibits a dual-resonant response with two well-defined impedance-matched bands centred at approximately 28 GHz and 39 GHz. Then, the substrate height, feedline width, patch sizes and the slot geometries (Slots 1–4) are all optimized in a full parametric way, yielding the reflection coefficients of the antenna to be around −38 dB and −52 dB at the two resonant frequencies, respectively. Both values are under the usual -10dB impedance matching criterion, confirming the high impedance matching and stable resonant performance over the desired operating bands. The corresponding realized gain response is shown in Fig. 4(b), which has two peaks of approximately 7.45 dBi at 28 GHz and 7.4 dBi around 36-37 GHz, and a local minimum of around 5.4 dBi near 31 GHz, indicating a temporary degradation of the radiation performance between the two operating bands. The dual-band nature defines the basic resonant behavior of the proposed single-element antenna, which is the basis for the two- and four-element MIMO configurations that are developed later, preserving and further improving this behaviour.

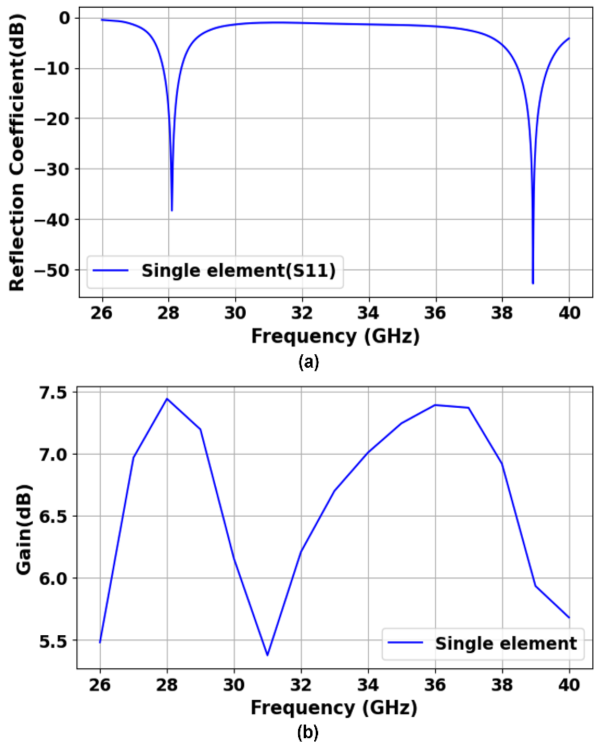

Figure 4. (a) Reflection coefficient and (b) Gain of proposed Single-element MIMO antenna.

3.2 Two Element Antenna Design

3.2.1 Orientation-Based Isolation in 2-Port MIMO

The single element antenna was extended to a 2-port MIMO configuration by considering three element orientations, parallel, anti-parallel and orthogonal, while keeping the same substrate as the single element design. The angular positioning directly influences inter-element coupling, radiation pattern orthogonality and spatial correlation [19]. Hence, orientation optimization is critical for port isolation, gain, diversity performance and signal decorrelation in compact space-constrained systems [20]. Figure 5(b), (d) and (f) show the reflection coefficients (S_{11}) for parallel, orthogonal and anti-parallel configurations respectively. All three configurations showed almost identical dual-band operation at 28.1 GHz and 38.992 GHz with only slight variations in return loss, showing that orientation has little impact on impedance matching. But the analysis of transmission coefficient (S_{12}, S_{21}) showed obvious differences in isolation. The parallel configuration gave 31 dB at 28 GHz and 25 dB at 38 GHz compared to the orthogonal configuration (30 dB and 19 dB) and against the anti-parallel configuration (25 dB and 21 dB) respectively, being up to 6 dB better at the higher band. This improvement can be attributed to the orthogonal arrangement that reduces the overlapping of the current distributions of the element and the matching of their radiation patterns to reduce the mutual coupling in the dominant polarization direction. Therefore, the parallel arrangement offers the best isolation between elements, while maintaining the performance consistent in both target bands, and was chosen as the configuration for the following MIMO development.

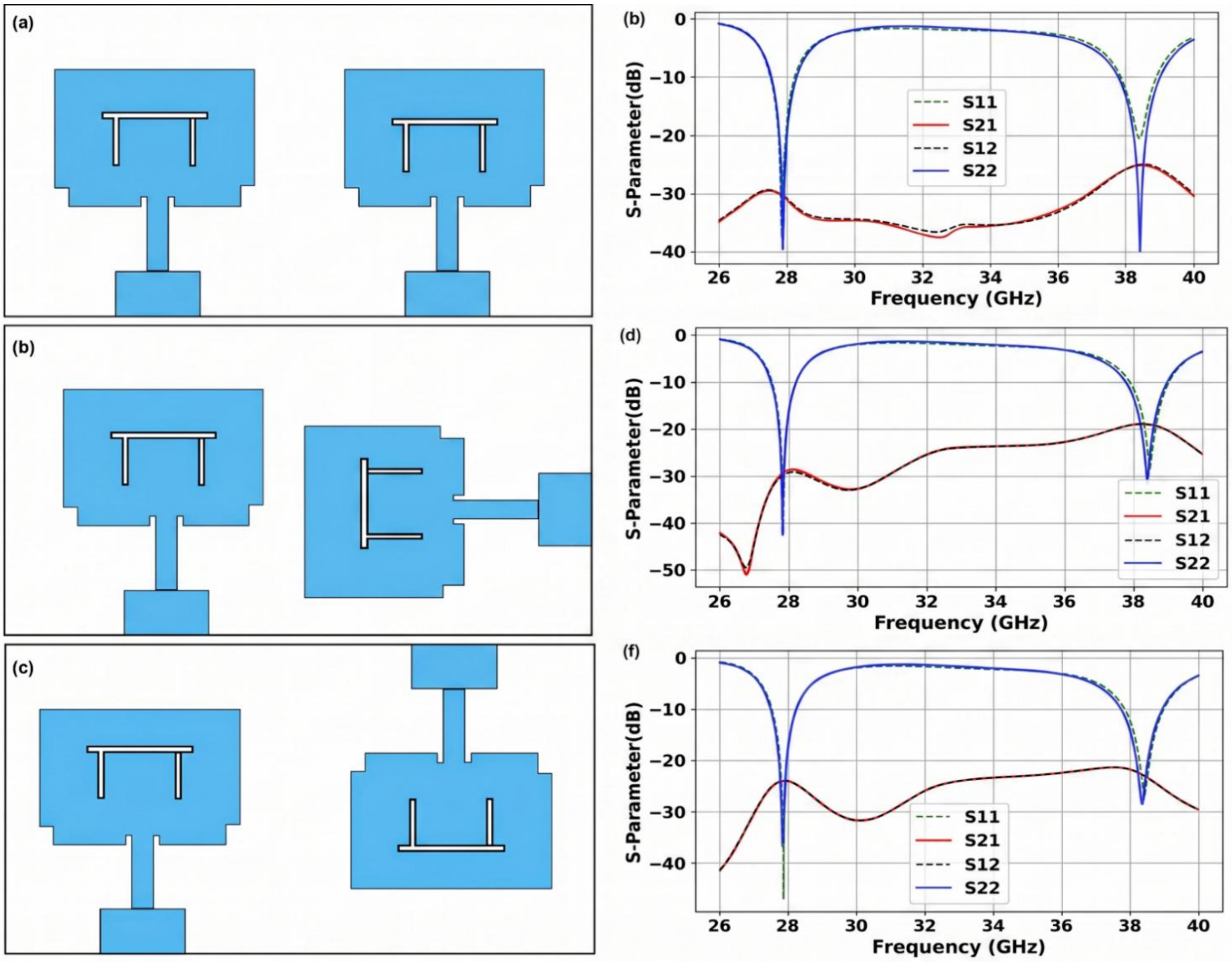

Figure 5. Comparative analysis of 2-Port MIMO configurations (a,b) Parallel design and S-parameter (c,d) Orthogonal design and S-parameter (e,f) Anti-parallel design and S-parameter.

3.3 Proposed Four Element MIMO Antenna

The best inter-element isolation in the 2-port analysis was shown by the parallel (side-to-side) configuration; thus the proposed four-element design is developed by combining two optimized 2-port MIMO pairs in this orientation. The front and back views of the proposed 2×2 MIMO antenna system with four number of π-slotted elements at 28 GHz and 38 GHz are shown in Fig. 6(a) and Fig. 6(b). Each element uses a separate ground quadrant of about 7.2 mm × 7.2 mm, separated from the adjacent quadrants by a cross-shaped gap of 1.42 mm width and arm length of 7 mm, which reduces the common surface-current paths between elements and improves inter-element isolation. All four elements are fabricated on a common substrate with a compact overall footprint of 15.82 mm x 15.82 mm. Two elements are placed parallel with an edge-to-edge separation of 3.58 mm, while the other two are placed with vertical separation of 2.51 mm from the first two in anti-parallel manner to reduce the electromagnetic coupling and improve the pattern diversity. The configuration exhibits excellent four-port MIMO performance in an ultra-compact footprint, with low ECC, high port-to-port isolation, and stable radiation characteristics, suitable for dual-band mm-wave 5G applications at 28 and 38 GHz. The simulated performance of the proposed four-element MIMO antenna is depicted in Figure 7.

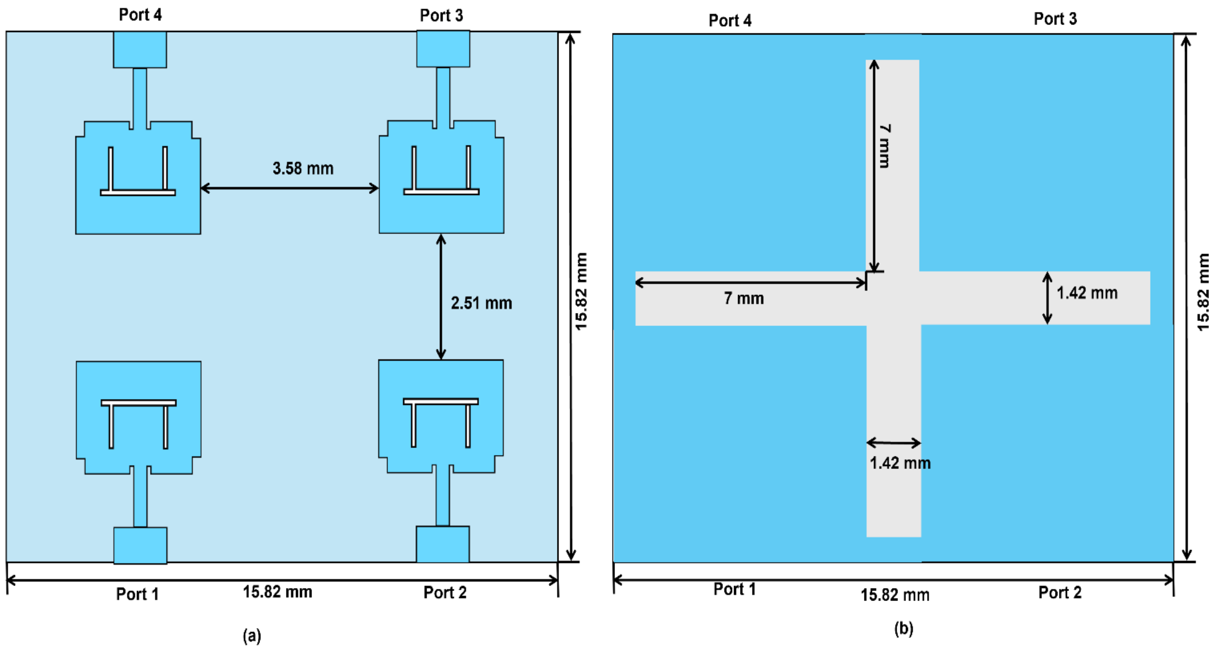

Figure 6. (a) Front and (b) Back view of proposed four-element MIMO antenna.

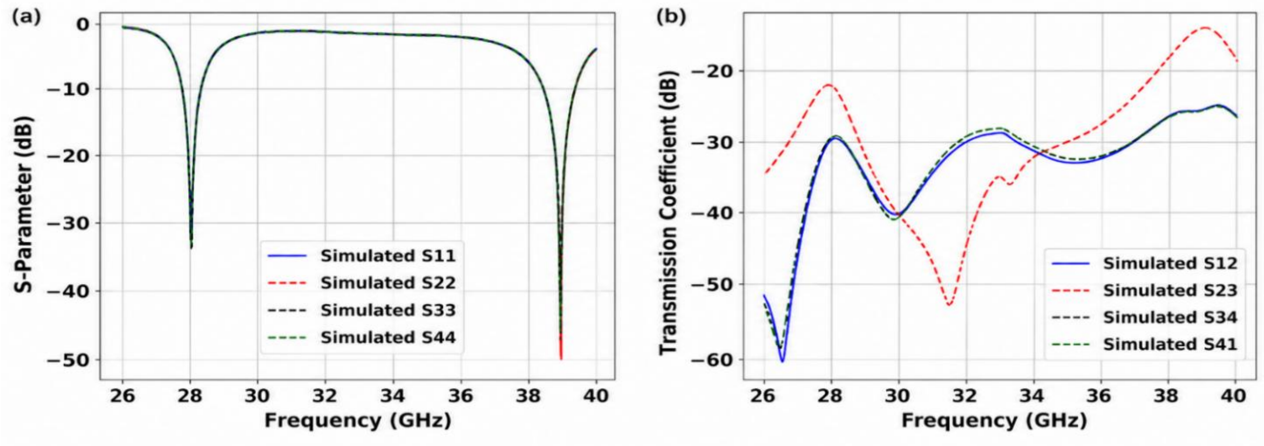

Figure 7. (a) Reflection coefficient and (b) Transmission coefficient of proposed four-element MIMO antenna.

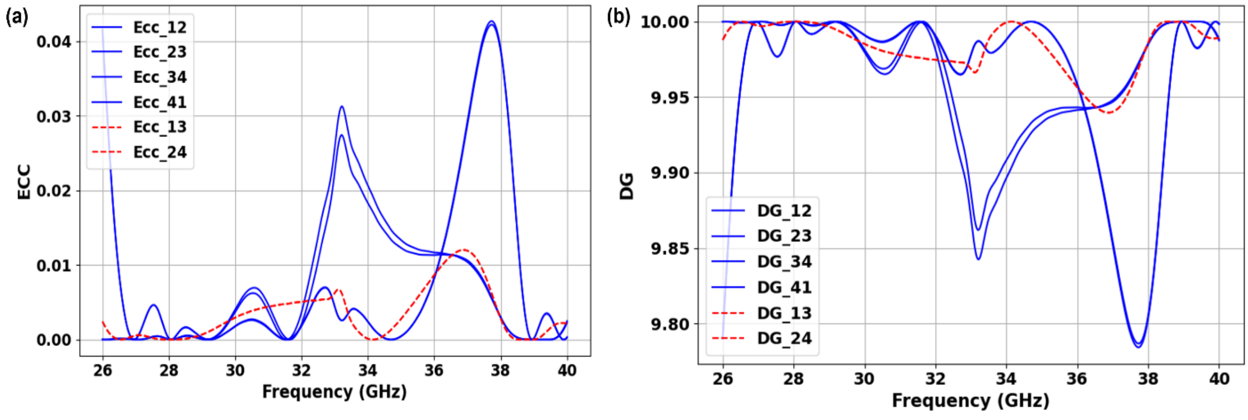

Figure 8. Simulated (a) ECC and (b) DG of the proposed 4-element MIMO antenna.

Figure 7(a) shows the reflection coefficients (S_{11}, S_{22}, S_{33}, S_{44}) showing good impedance matching with two resonances around 28 GHz and 38-39 GHz. The first resonance has return loss greater than -35 dB, the second resonance has return loss greater than -45 dB and all four ports have return loss below -10 dB in each operating band. The transmission coefficients (S_{12}, S_{23}, S_{34}, S_{41}) are shown in Figure 7(b) for the mutual coupling between the element pairs. Three pairs of coupling start below –50 dB near 26 GHz. One pair (S_{23}) start near –35 dB. Isolation is better than –30 dB for all port combinations at both 28 GHz and 38 GHz bands. The dual-band isolation performance validates the proposed four-port π-slotted MIMO antenna's suitability for 5G applications at 28 and 38 GHz with low mutual coupling, enhanced diversity performance, and improved channel capacity.

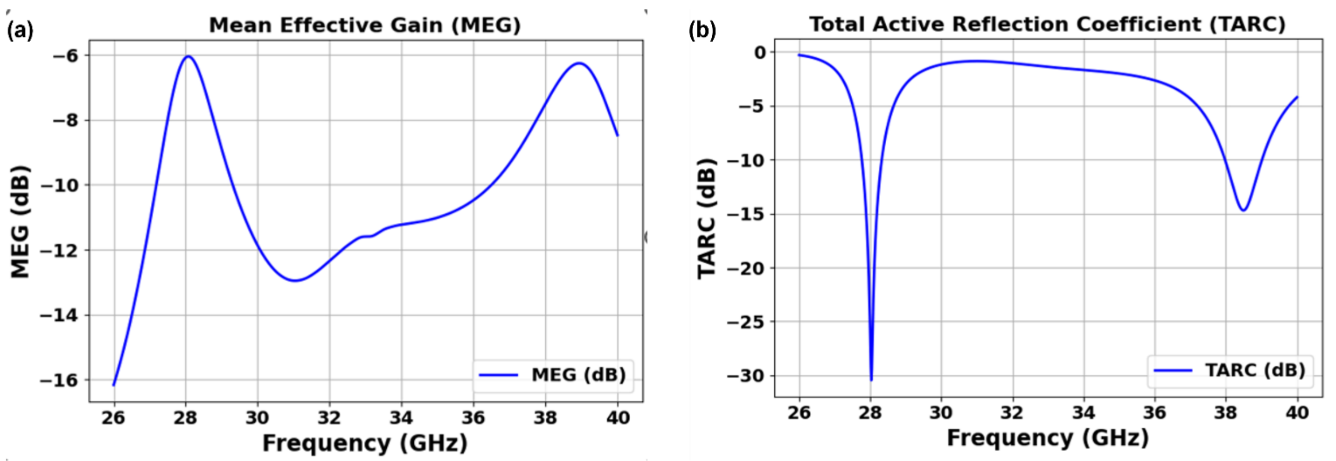

Figure 9. Simulation result of (a) MEG and (b) TARC of the proposed 4-element MIMO antenna.

3.4 Four-Element MIMO Performance Parameters

3.4.1 ECC, DG

The envelope correlation coefficient (ECC) is an important parameter in the design of π -slotted MIMO antennas, which measures the correlation between the antenna elements and their channels. It is mainly based on the similarity of the radiation pattern e.g. the orthogonal polarization elements give a near-zero ECC [21]. Ideally, ECC should be minimized to maximize the channel capacity and diversity gain. However, practical factors such as mutual coupling and fabrication limitations prevent perfect decorrelation, so ECC < 0.5 is acceptable for effective performance. In practice, ECC is easily evaluated using S-parameters obtained from simulations or measurements, thus bypassing the need to perform a complex far-field analysis, and is calculated using Eq. (5).

$$\text{ECC}=\frac{|S_{11}^{*}S_{12}-S_{21}^{*}S_{22}|^2}{(1-|S_{11}|^2-|S_{21}|^2)(1-|S_{22}|^2-|S_{12}|^2)} \quad (5)$$

As shown in Figure 8(a), the ECC of all antenna pairs (ECC_{12}, ECC_{23}, ECC_{34}, ECC_{41}, ECC_{13} and ECC_{24}) is evaluated over 26–40 GHz. The proposed four-element pi-slotted MIMO antenna shows very low ECC values less than 0.05 over the band and most of the values are near to < 0.01. The minor peaks at ~33 GHz (~0.03) and ~38 GHz (~0.045) are still well below the threshold of 0.5, showing excellent isolation and pattern decorrelation. This indicates a high degree of channel independence which allows for strong spatial diversity and better capacity for dual band 5G millimeter wave applications.

The diversity gain (DG) is a key metric that indicates a MIMO system's capability to cope with fading and guaranty reliable communication in multipath environments [22]. Higher DG values mean better signal quality and channel capacity, with optimum performance nearing 10 dB. Since DG is inversely related to ECC, the lower the correlation between antenna elements, the higher the diversity gain. This shows the importance of strong isolation and pattern diversity. For realistic 5G mm-wave systems, it is preferable to have DG values greater than 9.95 dB. The DG is calculated as:

$$\text{DG}=10\sqrt{1-ECC^2} \quad (6)$$

Figure 8(b) shows the DG of all antenna pairs from 26-40 GHz. In the proposed antenna, the DG values are around 10 dB over the band, except slight drops to ~9.8-9.85 dB around 33 GHz and 38 GHz. These results, together with the low values of ECC, confirm the excellent diversity performance and reliable multi-stream transmission for 5G applications at 28/38 GHz.

3.4.2 MEG, TARC

The Mean Effective Gain (MEG) evaluates the average received power of a MIMO antenna element in a multipath environment relative to an isotropic radiator, incorporating radiation efficiency, pattern diversity, and polarization effects [23]. For a 4-element system, the MEG of port *i* is derived from S-parameters as:

$$MEG_i=\frac{1}{2}(1-\sum_{j=1}^{2}\left|S_{ij}\right|^2 \quad (7)$$

Figure 9(a) shows the MEG of the proposed four-element MIMO antenna in the operating band. The MEG values are close to the ideal value of −6 dB with peaks around the resonant frequencies of 28 GHz and 39 GHz. Slight deviations above –6 dB indicate good power balance between ports and efficient radiation. In conclusion, the results show that the system can receive energy effectively, achieve strong diversity performance, and operate reliably for dual-band 5G mm-wave applications.

The Total Active Reflection Coefficient (TARC) is a more comprehensive measure for the performance of multi-port MIMO systems, as it takes into account the port reflections and the mutual coupling for simultaneous excitations with arbitrary phases, thereby providing a more realistic assessment compared to the conventional S-parameters [24]. It is defined as:

$$\text{TARC}=\frac{\sqrt{\sum_{i=1}^{N}\left|\sum_{j=1}^{N}S_{ij}a_j\right|^2}}{\sum_{i=1}^{N}|a_i|^2} \quad (8)$$

Where, S_{ij} = S-parameter from port j to port i, a_i = excitation amplitude/phase applied at port i.

Figure 9(b) shows the TARC over 26–40 GHz, exhibiting strong dual-band performance at 28 GHz and 38–39 GHz. The TARC reaches ~–30 dB at 28 GHz and ~–14 dB at 39 GHz, while remaining below –10 dB across most of the band. These low values indicate minimal reflected power and efficient radiation under simultaneous multi-port excitation, confirming the antenna's suitability for dual-band 5G mm-wave applications.

3.5 Proposed Four Element MIMO Antenna

The single, two and four element MIMO antenna configurations are compared in Figures 10(a), (b) and (c). From Figure 10(a), it can be seen that all the designs have different dual-band resonance around 28 GHz and 38 GHz. The proposed four elements array shows a remarkable improvement in the return loss performance (below −40 dB) indicating an effective impedance matching than the single and two elements configuration. The gain performance is increasing with the number of elements which is shown in Figure 10(b). The single-element antenna provides moderate gain, which is improved in the two-element design and reaches about 8.5 dBi at 28 GHz in the proposed four-element configuration. Such an improvement is attributed to a higher directivity and a constructive coupling among elements. Figure 10(c) shows the radiation efficiency of the proposed antenna for the operational frequency bands. The efficiency is consistently over 90% for all configurations, with the 4 element array having an exceptionally high efficiency of ≥95% in both the 28 GHz and 38 GHz bands.

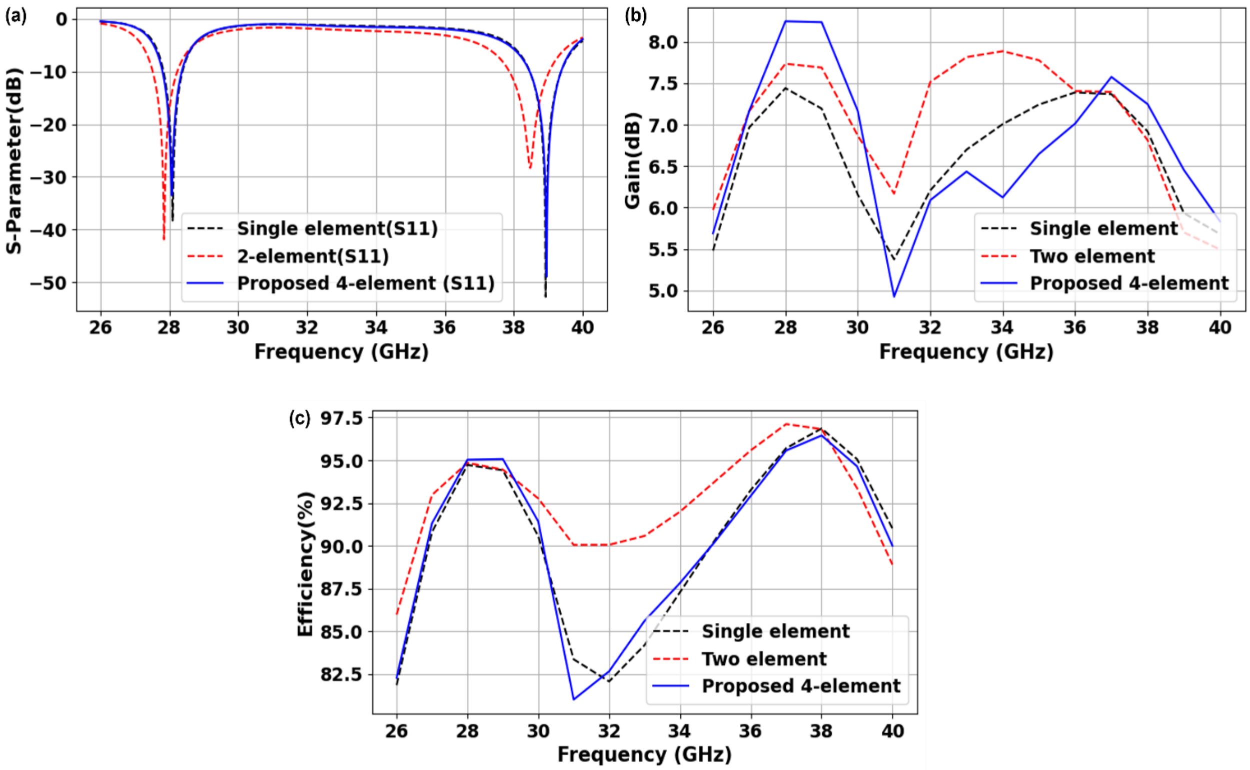

Figure 10. Comparison between 1, 2 and 4-element antenna: (a) S-parameter (b) Gain (c) Radiation efficiency.

This leads to low power losses despite the increased structural complexity and inter-element interactions. The results indicate that the impedance matching and gain are greatly improved by scaling from single-element to four-element configuration. The presented design can be considered as a promising candidate for dual-band 28/38 GHz 5G mm-wave applications.

3.5 Radiation Pattern of 4-Port MIMO Antenna

The radiation pattern is a description of the spatial distribution of power radiated by an antenna. It shows how electromagnetic energy is emitted in different angular directions in three-dimensional space [25]. It gives fundamental insight into antenna directivity, gain, beamwidth, polarization characteristics and coverage capabilities, and is thus a key metric for assessing the antenna performance in practical wireless communication systems [26]. Figure 11 shows the simulated two-dimensional radiation patterns of the proposed four-element π -slotted MIMO antenna in E-plane and H-plane at 28.072 GHz and 38.95 GHz. The patterns of all four elements are overlaid showing the pattern diversity and spatial coverage capability of the antenna. The E-plane patterns show frequency dependent variations in directivity over the two operating bands as shown in Figs. 11(a) and 11(b). At 28.072 GHz, the radiation characteristics exhibit a highly directional pattern, with all four elements generating well-defined, closely overlapping main lobes toward approximately 5°, indicating a high degree of beam consistency and focused radiation. At 38.95 GHz, the E-plane patterns are slightly more diversified among the elements, with main lobes shifting toward 7° and mild broadening, which is consistent with the natural evolution of radiation behavior at higher frequencies. Nevertheless, the overall pattern structures are stable, preserving clear directivity and consistent polarization across the MIMO elements. The radiation patterns shown in Figures 11(c) and 11(d) indicate that the E-plane is quite uniform over all elements whereas the H-plane presents significant pattern diversity, which is beneficial for MIMO spatial multiplexing and diversity gain. At 28.072 GHz the H-plane shows symmetrical main lobes, while at 38.95 GHz the asymmetry and small side lobes increase, providing a wider angular coverage and better spatial diversity. These results confirm that the proposed four-port MIMO antenna has steady radiation characteristics against frequency and is suitable for multi-band 5G mm-wave applications with dependable spatial performance.

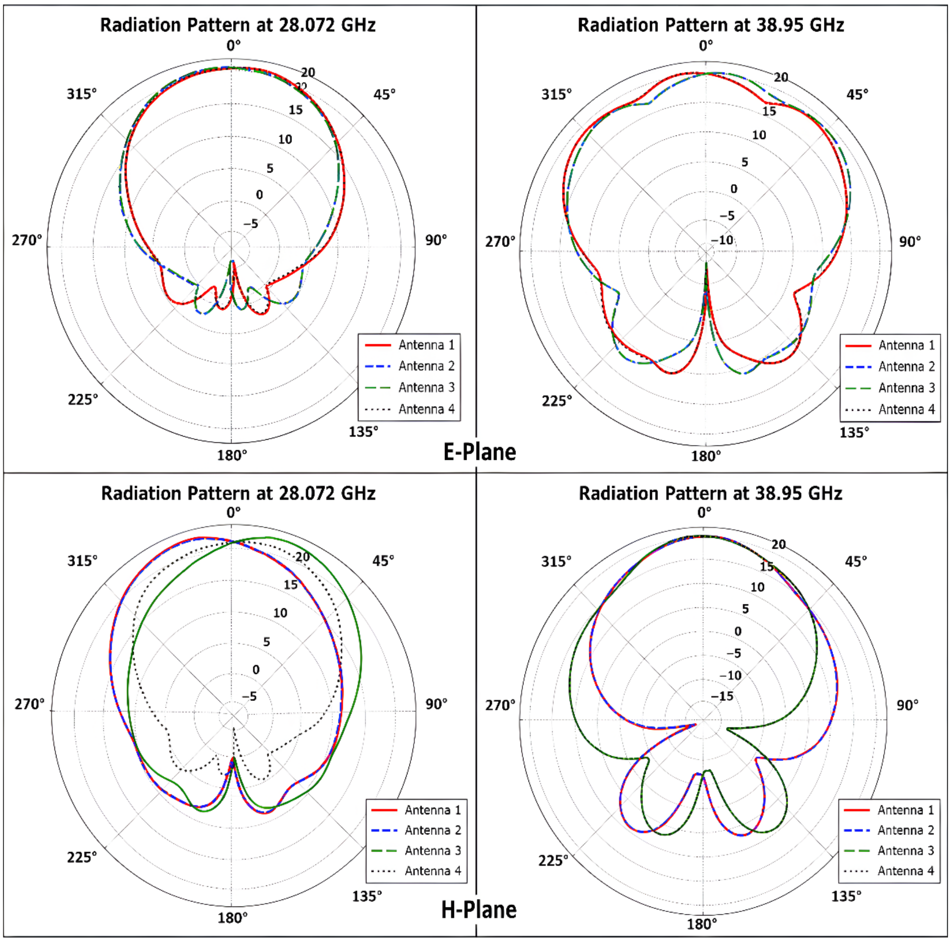

Figure 11. Simulated E-Plane (a, b) and H-Plane (c, d) radiation patterns at 28.072 GHz and 38.95 GHz.

4. MACHINE LEARNING ANALYSIS

The electromagnetic performance of the proposed four-element MIMO antenna, including its gain, isolation, bandwidth, efficiency, and diversity characteristics, was achieved through the proposed slot geometry, substrate selection, and decoupling structure, optimized via full-wave simulation in CST Microwave Studio. This section presents a separate, complementary contribution: the integration of a machine learning (ML) regression framework, trained on the CST-generated dataset, to enable rapid and computationally inexpensive prediction of these performance metrics for new or unseen design configurations. The ML models described below were not used to modify or optimize the antenna geometry; rather, they serve as a post-design surrogate model that estimates performance outcomes without requiring repeated full-wave simulation [27]. Such surrogate modelling is a well-established practice in antenna engineering, where a dataset generated from full-wave simulations is used to build models capable of capturing complex, nonlinear relationships among design parameters and performance metrics such as bandwidth, gain, efficiency, and isolation [28], [29]. Consequently, once the antenna geometry has been established through EM design, the ML framework facilitates fast, low-cost performance prediction, offering a practical alternative to repeated parametric sweeps for design-space exploration and rapid what-if analysis. This framework supports efficient post-design evaluation of the proposed antenna for dual-band 28/38 GHz 5G mm-wave applications.

The structured ML workflow for predicting the performance of the 4-element MIMO antenna after the electromagnetic design is illustrated in Fig. 12. The process starts with the data collection from CST parametric sweeps, then pre-processing steps like data cleaning, normalization, feature selection etc. are performed to prepare an optimized dataset for ML modeling. Then the cleaned data is split into 80%

training and 20% testing to ensure the evaluation is not biased. To make a full comparison, we trained several regression algorithms on the same dataset: Linear Regression, Decision Tree, XGBoost, Extra Trees, Random Forest and K-Nearest Neighbors (KNN). Model performance is assessed using MAE, MSE, and R^2 metrics, allowing robust benchmarking across algorithms. The best-performing model is then used to predict the antenna's gain; predictions are compared with CST results, and if the error exceeds 5%, the workflow returns to the regression training stage to minimize prediction error. At no stage does this workflow feed back into or alter the antenna's physical geometry.

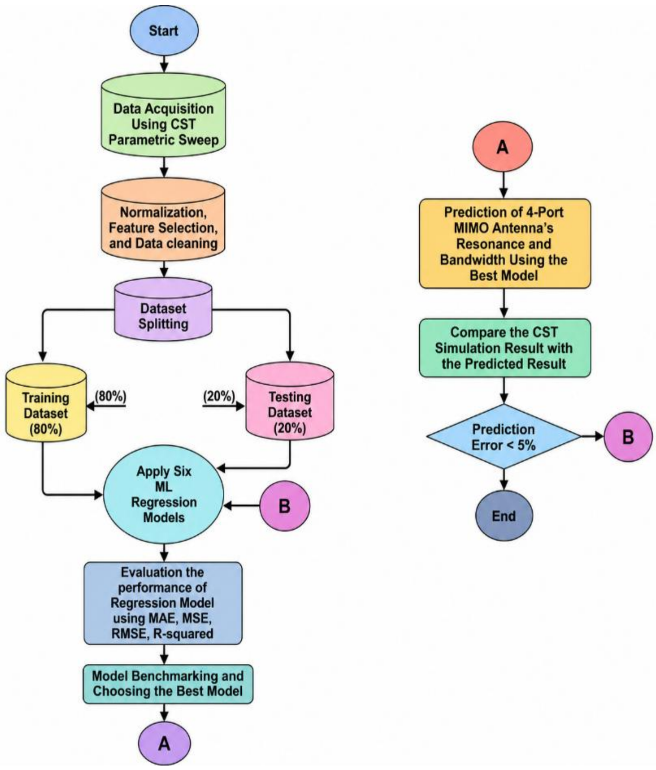

Figure 12. ML-driven performance analysis of the proposed 4-element MIMO Antenna.

4.1 Dataset Generation and Pre-processing

The dataset of the four-element MIMO antenna is generated using the CST Microwave Studio software by conducting systematic parametric sweeps of the important design parameters. The S-parameters and gain were recorded for each configuration and exported as CSV/Excel files for further processing in Python. The raw data were then cleaned by removing duplicates and missing values, restructured into a consistent input-output format, and normalized using Min-Max scaling to the range [0, 1]. An 80–20 train–test split was used to guaranty reliable model evaluation and generalization to unseen configurations. A total of 193 samples were generated to capture the nonlinear electromagnetic behavior of the antenna across the design space with sufficient variability. Table 2 summarizes the 19 floating-point parameters of each sample, which include important geometric variables such as the geometric dimensions of the four slot elements (SW_1, SL_1, W_2, L_2, W_c, W_L, W_m, L_m), length from center of coordinate to slot-1 and slot-2 (PL,PW), feeding line width specifications (W_f, L_f), and key metrics for performance: resonant frequencies (F_1, F_2), return loss (RL_1, RL_2), and realized gain (G_1, G_2) for the 28 GHz and 38 GHz operating bands. These features together constitute a comprehensive and well-structured dataset that can serve as a strong basis for accurate ML-based modeling and prediction of the proposed MIMO antenna performance.

4.2 Dataset Statistical Characteristics

The ML model development is founded upon a comprehensive dataset comprising 193 samples derived from rigorous CST electromagnetic simulations, systematically capturing the complex electromagnetic characteristics and performance behavior of 4-element MIMO antenna across its operational frequency spectrum. The dataset underwent comprehensive pre-processing, including normalization for consistent scaling and outlier removal to eliminate anomalies, ensuring enhanced model reliability and training accuracy. Following pre-processing, statistical analysis using histograms was conducted to examine distributions and relationships between design features and performance metrics for the 28 GHz and 38 GHz bands. Figure 13 presents these histograms for all input design parameters and output performance metrics of the 4-element MIMO antenna.

Table 2. Dataset characteristics and purpose

Feature	Specification	Purpose
Dataset Size	193 samples × 21 columns	Generated using CST parametric sweep.
Training/ Testing	Training=154(80%), Testing=39 (20%)	Enables reliable training and unbiased evaluation.
Input Parameters	13 inputs=SW_1, SL_1, W_2, L_2, W_c, W_L, W_m, L_m, W_f, L_f, W_T, PL, PW	Controls antenna structure and directly impacts performance.
Output Parameters (Performance)	6 outputs= F_1, F_2, RL_1, RL_2, G_1, G_2	Essential for building relationship with input parameters

4.3 Dataset Preparation, Pre-processing, and Model Configuration

The data set was first processed before the modeling phase through a series of processes such as removing outliers, normalizing the data, selecting features, and setting hyperparameters.

Outlier removal: Outliers or non-physical data points were detected in the data set, which could arise from convergence problems in electromagnetic model simulations. Outliers were identified using the interquartile range (IQR) criterion (i.e., samples with output values falling outside 1.5×IQR of the first and third quartiles were flagged). Samples with physically inconsistent responses were excluded from further analysis, removing 5 samples from the original dataset. Feature selection: The input variables were selected according to their physical relevance to the electromagnetic behavior of the proposed antenna, as supported by the parametric and sensitivity analyzes presented in Section 3. Predictors were restricted to geometrical parameters that have a direct impact on the resonant frequency, impedance matching, inter-element coupling and gain. Thus, 13 geometrical parameters were selected as the final input features, and the parameters which had an insignificant influence during the parametric analysis were discarded.

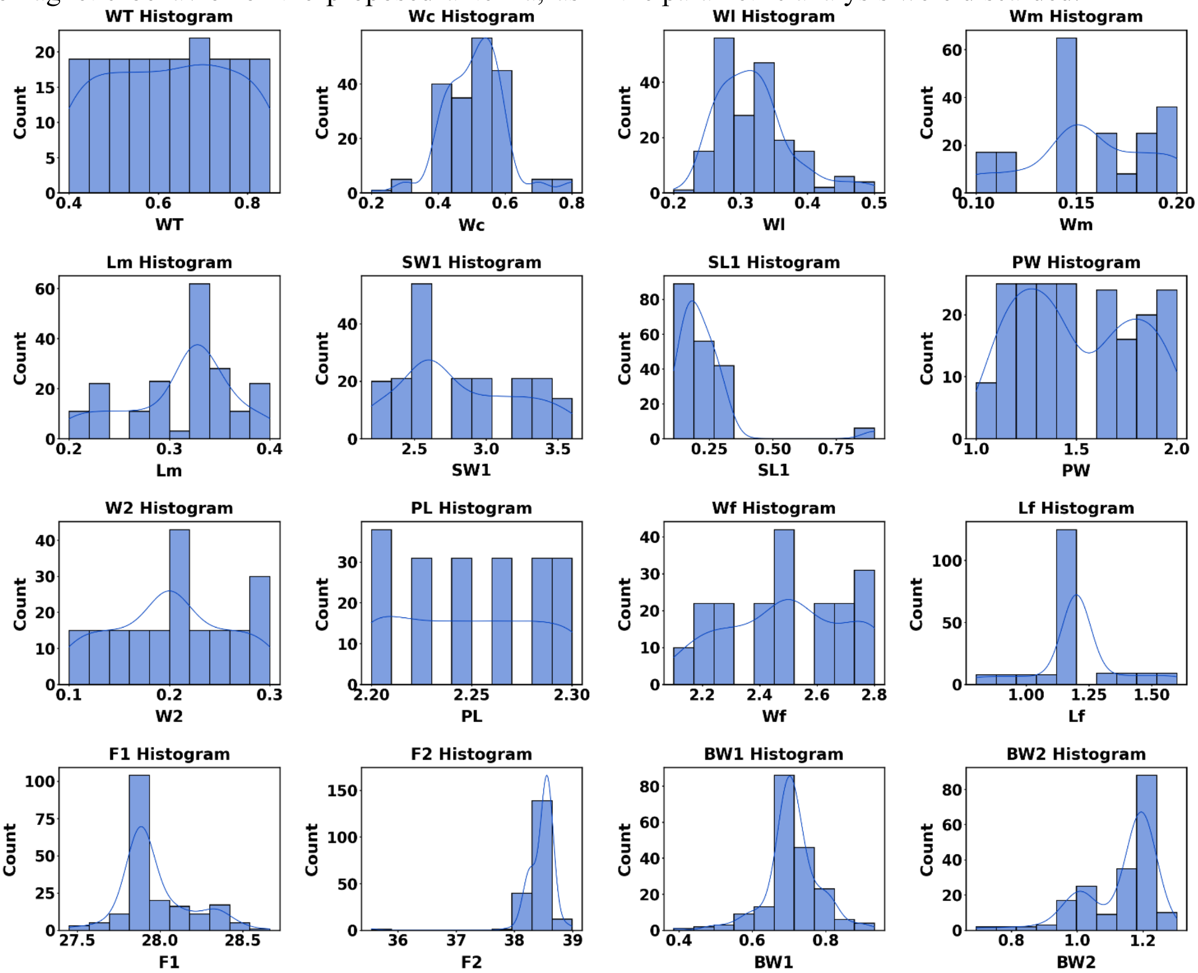

Figure 13. Histogram visualization of design features and output metric distributions of the generated dataset.

Hyperparameter configuration Six regression algorithms were explored: Linear Regression (LR), Random Forest Regression (RFR), Decision Tree Regression (DTR), Extra Tree Regression (ETR), XGBoost Regression (XGBR) and K-Nearest Neighbors Regression (KNN). For the tree-based models (RFR, DTR and ETR), the main hyperparameters were the maximum depth of the tree, the minimum number of samples required to split an internal node, and the minimum number of samples required to be at a leaf node, while RFR also used the number of estimators ((n_estimators)). The main parameters of XGBR were learning rate, maximum depth and subsample ratio, (n_estimators). The KNN model was trained according to the number of nearest neighbors, distance metric and weighting strategy. LR was used as a baseline model to compare with the nonlinear regression methods. Hyper-parameters were selected using [default settings/manual tuning/grid search/randomized search with k-fold cross-validation] with a fixed random_state = [value] for all stochastic algorithms (when applicable) to ensure reproducibility across multiple runs.

4.4 Overview of ML-Based Regression Models

Based on detailed statistical analysis of antenna design dataset discussed in previous subsection, this subsection explores several ML regression techniques that are suitable for prediction of performance indicators and optimization of 4-element MIMO antenna design. The complex relationship between the design parameters and the antenna behavior at the targeted 28 GHz and 38 GHz frequency bands is modeled using six regression models. The aim is to assess the performance, precision, and interpretability of these methods. We chose ML regression models for their transparency and computational efficiency which are necessary for applications where the interpretability of the model and a clear mapping between parameters and performance are needed. The detailed description of each regression model is given below to establish a thorough comprehension of their underlying mechanisms and suitability for optimization of the antenna design. Linear regression is a basic statistical modeling technique that uses mathematical optimization to find direct linear relationships between the dependent performance variables and one or more independent design parameters [30]. The method minimizes the residuals between the observed and predicted values using the least squares, resulting in a best-fit linear model that captures essential parameter-performance relationships for antenna design. The regression model is described by the Eq. (9).

$$Y=\beta_0+\sum_{i=1}^{n}\beta_i x_i + \varepsilon \quad (9)$$

Where β_0 is the intercept, β are regression coefficients, and ε denotes the error term.

Decision Tree Regression splits the dataset based on input features using a hierarchical structure generated by recursive binary splitting [31]. Each core node represents a threshold or decision rule, and each leaf node represents a numerical forecast. This approach allows to model nonlinear relationships and interactions between variables while maintaining a high level of interpretability. A Decision Tree Regression equation is a piecewise constant function in the form of a prediction being the average of the target value in the region defined by a sequence of if-then conditions on input features. Mathematically, if a data point x reaches a leaf node l, the prediction is given by Equation (10).

$$\hat{y}\,(x)=\frac{1}{N_l}\sum_{i\epsilon L} y_i \quad (10)$$

Here, $\hat{y}\,(x)$ is the the predicted value for the data point x, N_l is the number of data points in leaf node l, L is the set of indices of the data points in leaf node l and y_i is the target value for data point i.

Random Forest Regression is a powerful ensemble learning method that improves prediction accuracy and generalization by constructing numerous decision trees during training and combining their outputs [32]. Through the use of bootstrap aggregation (bagging) and feature randomness, it successfully minimizes overfitting, a problem that is frequently encountered in single decision tree models and produces consistently stable and dependable predictions over a broad range of antenna design parameter choices. Random Forest regression is defined by Eq. (11).

$$\hat{y}=\frac{1}{T}\sum_{t=1}^{T} f_t(x) \quad (11)$$

Here, $f_t(x)$ represents the prediction from the t^{th} decision tree, and T is the total number of trees.

Extra Trees Regression (ETR) is an ensemble learning technique which extends Random Forest by injecting full randomness in the choice of split point, removing the search for the optimal threshold at each node and instead choosing split points randomly for given features [33]. This enhanced randomization approach significantly decreases model variance and overfitting, while improving stability and generalization performance. It is especially beneficial for high-dimensional antenna design datasets with inherent noise and complex parameter interactions. The ETR is an ensemble of M randomized decision tree and is defined in Eq. (12).

$$\hat{y}\,(\mathrm{x})=\frac{1}{M}\sum_{m=1}^{M} f_m(x) \quad (12)$$

Here, $\hat{y}$ (x) is final predicted output, $f_m(x)$ is prediction of the m^{th} decision tree and M is total number of trees in the ensemble.

XGBoost Regression is a popular gradient boosting algorithm, which is known for high accuracy, speed and efficiency. An ensemble of decisions trees is built sequentially, where each new tree corrects the errors of the previous ones by minimizing a defined loss function [34]. The XGBoost algorithms can be effectively utilized by antenna engineers in computational simulation data and experimental measurements to predict the important antenna performance parameters such as directivity, gain, and radiation pattern characteristics that can facilitate improved design optimization and accurate performance prediction in the development of electromagnetic systems. The XGBoost Regression can be represented as Eq. (13).

$$\mathcal{L}^{t} = \sum_{i=1}^{n}[l(y_i, \hat{y}_i^{(t-1)}\text{-}f_t(x_i))+\Omega\,(f_t) \quad (13)$$

Here, $l(y_i, \hat{y}_i)$ is the differentiable loss function, $f_t(x_i)$ is the new tree added at iteration t, $\Omega\,(f_t)$ is the regularization term that penalizes model complexity.

K-Nearest Neighbors (KNN) Regression is a non-parametric approach where the output of an input is predicted by the average of the target values of the k nearest neighbors of the input in the feature space [35]. It does not make any assumptions about the underlying data distribution so it can capture complex, nonlinear relationships. When similar design configurations result in similar results, KNN can be useful for fast approximations in antenna design. However, it suffers from the curse of dimensionality in high dimensional spaces, and is sensitive to the choice of k and distance metric. Typically, the Euclidean distance between a test sample x and each training sample x_i is given by Eq. (14) for finding the k nearest neighbors.

$$\mathrm{d}\,(\mathrm{x}, \mathrm{x_i})= \sqrt{\sum_{j=1}^{n}(x_j - x_{ij})^2} \quad (14)$$

Here, x = feature vector of the test sample, x_i = feature vector of the i^{th} training sample and n = number of features.

4.5 Evaluation Metrics for Model Performance

The Selection of regression models. Evaluation metrics provide important quantitative measures for measuring the accuracy, reliability and generalization capacity of predictive models. Prediction errors are quantified in different scales and units using important metrics like Mean Absolute Error (MAE), Mean Squared Error (MSE), Root Mean Squared Error (RMSE) to give a more complete picture of model precision. R-Squared

(R^2) and Variance Score supplement the above by measuring how well the model captures the variance in the target data, with higher values signifying better predictive ability and a better fit to the underlying data distribution.

MAE is a regression evaluation metric which measures the mean of absolute difference between predicted and actual values. It provides a simple measure of prediction accuracy which is less sensitive to outliers compared to squared error metrics [36]. It is defined mathematically in Eq. (15).

$$MAE = \frac{1}{n}\sum_{i=1}^{n}|\hat{y_i} - y_i| \quad (15)$$

Where, $\hat{y_i}$ and y_i are the predicted value and actual value respectively, and n is the number of samples.

MSE is a standard metric for regression evaluation, which captures the average of the squared difference between the predicted and true values. Thus, it offers an overall indicator of prediction accuracy, while the higher the error, the more penalty it gets due to the square operation [37]. The mean square error is given by Eq. (16)

$$MSE = \frac{1}{n}\sum_{i=1}^{n}(\hat{y_i} - y_i)^2 \quad (16)$$

The RMSE is the square root of the mean of the squared deviations between predictions and observations [51]. It indicates larger errors and provides a clear indication of prediction accuracy in the same units as the target variable. Eq. (17) depicts the RMSE.

$$RMSE = \sqrt{MSE} = \sqrt{\frac{1}{n}\sum_{i=1}^{n}(\hat{y_i} - y_i)^2} \quad (17)$$

R^2 is a statistical metric that measures the proportion of variance in the dependent variable explained by the regression model with a range from 0 to 1 where a value of 1 is indicative of a perfect fit of the model with zero prediction error, and a value of 0 indicates that no variability in the target variable is explained by the model [38]. This basic evaluation metric is a measure of the effectiveness of the model, based on how well the independent design parameters capture the observed variation in the antenna performance characteristics and is mathematically formulated as shown in Eq. (18).

$$R^2 = 1 - \left(\frac{SSE}{SST}\right) \quad (18)$$

Here, SSE represents the total squared differences between predicted and actual values, while SST measures total dependent variable variation by summing squared differences between actual values and their mean.

The Variance Score is a regression evaluation metric that explains how much variance in the target variable is explained or accounted for your model. It measures the proportion of the total variation in the dependent variable that can be accounted for by the relationships represented by the independent variables in your model [39]. A score of 1 means a perfect prediction. Lower scores mean the model is unable to explain some of the variation in the data. The formula of variance score is shown in Eq. (19)

$$\text{Variance Score} = 1 - \frac{\mathrm{Var}(\hat{y_i} - y_i)}{\mathrm{var}(y)} \quad (19)$$

Here, $\hat{y_i}$ and y_i denote the predicted value and the actual value.

5. ANALYZING PREDICTION OUTCOMES FOR 4-PORT MIMO ANTENNA

5.1 Prediction of Bandwidth

Bandwidth prediction accuracy is a critical measure of the ML framework's reliability, as it determines how faithfully the surrogate model can reproduce the operational frequency range established by the antenna's electromagnetic design without requiring repeated full-wave simulation. Table 3 provides a detailed comparative analysis of six regression algorithms for predicting the two bandwidths (BW_1 and BW_2) of the proposed 4-element MIMO antenna, whose actual bandwidth values (0.6 GHz and 1 GHz, respectively) were determined by the EM design described in section 3. Among all the evaluated models, Extra Tree Regression achieved the best overall performance on prediction with the lowest error metrics and highest accuracy. It achieved MAE of 0.52% (BW_1) and 0.54% (BW_2) and R2 scores of 93.07% and 98.06%, respectively, indicating its strong ability to capture the nonlinear mapping between geometric parameters and bandwidth. BW2 had the least MAE (0.59%), MSE (0.03%), and RMSE (1.74%) with an R2 of 97.51% which also indicates the efficiency of Decision Tree Regression. KNN yields consistently good results on both bandwidths (R 2 of 90.67% and 97.22%) whereas Random Forest and XGBoost deliver robust but slightly less accurate. Linear Regression has a relatively higher error and lower R2 (67.66% for BW1, 83.17% for BW2) which is a reflection of its limited ability to model the nonlinear relation between the geometry and the bandwidth which is a characteristic of the antenna design and not of the antenna itself. The higher prediction accuracy of Extra Tree Regression is further shown in Figures 14(a)–(b) and Figure 15, confirming it as the most suitable predictive model for this dataset.

5.2 Prediction of Gain

Table 4 shows a comparison of six regression models to predict the gain values G_1 and G_2 of the proposed antenna, gain values that are the outcome of the physical design of the antenna and extracted directly from the CST simulation. Extra Tree Regression again has the highest prediction accuracy, R^2 94.14% (G_1) and 89.25% (G_2) and the lowest MAE (2.27% and 1.90%, respectively). Decision Tree Regression is also near (R^2 of 94.13% and 87.05%) and XGBoost performs well for G1 (R^2 = 94.04%). Random Forest and KNN show moderate accuracy (R^2 between 81-90%) while Linear Regression has poor performance (MAE of 37.16% and 12.60%; R^2 of 25.26% and 16.18%), confirming that the gain varies nonlinearly with the antenna's geometric parameters in a way that simple linear models cannot capture.

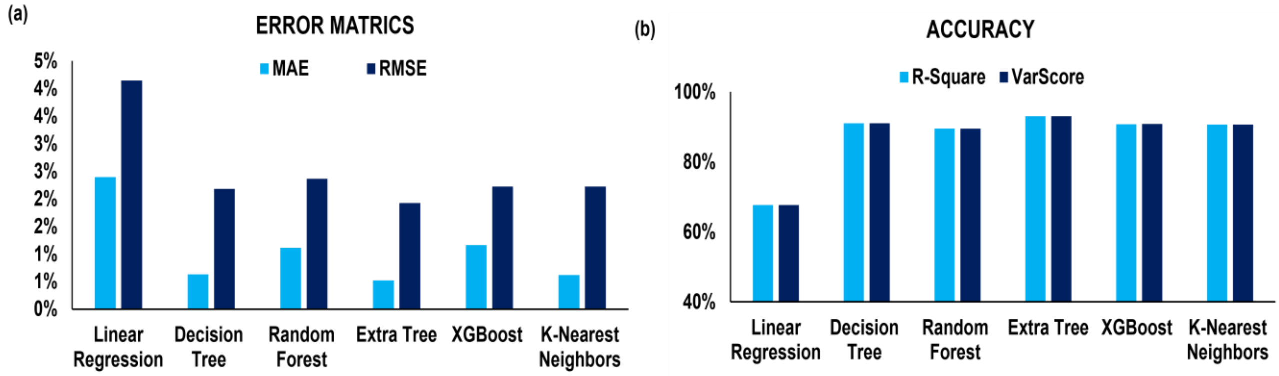

Figure 14. (a) ML error and (b) Accuracy analysis for bandwidth.

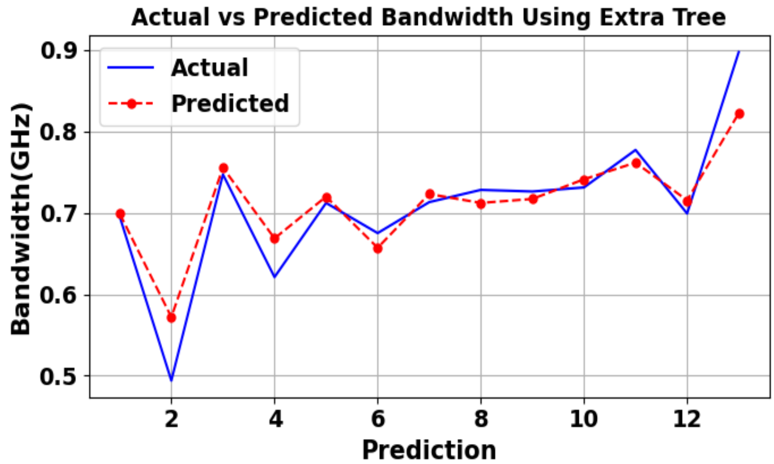

Figure 15. Actual vs. predicted 1st bandwidth using Extra Tree regression.

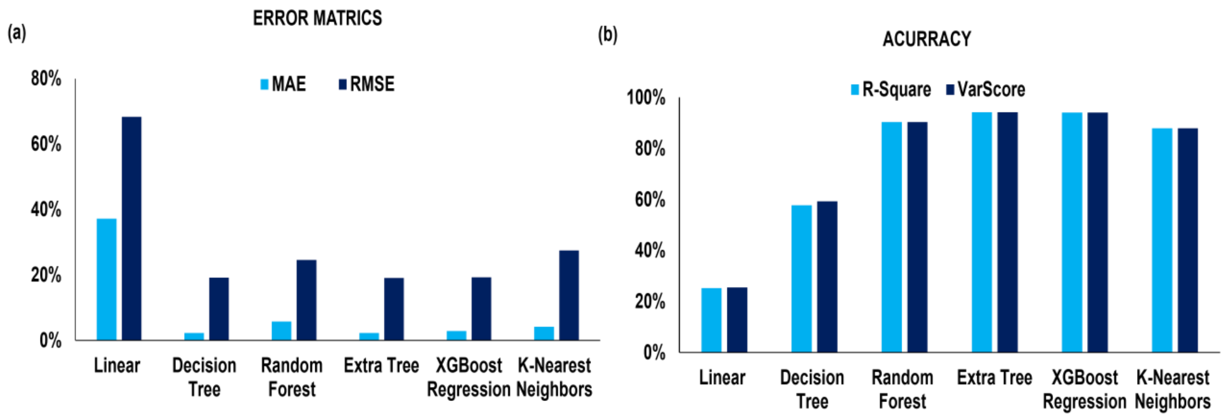

Figure 16. (a) ML error and (b) Accuracy analysis for gain

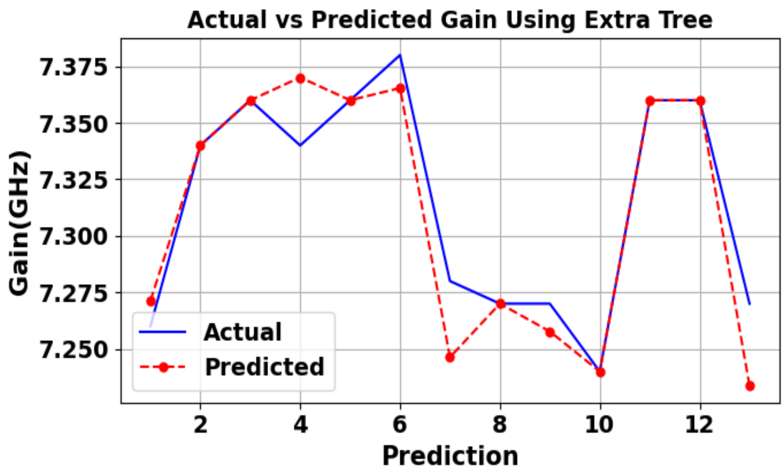

Figure 17. Actual vs. predicted 1st gain using Extra Tree regression.

Table 3. Bandwidth prediction performance.

Algorithms	Frequencies	MAE (%)	MSE (%)	RMSE (%)	R-Square (%)	Var Score (%)
Linear Regression	BW_1	2.39	0.17	4.14	67.66	67.72
	BW_2	2.92	0.21	4.53	83.17	83.17
Random Forest Regression	BW_1	1.11	0.06	2.36	89.47	89.51
	BW_2	1.19	0.04	2.02	96.66	96.68
Decision Tree Regression	BW_1	0.63	0.05	2.18	91.04	91.04
	BW_2	0.59	0.03	1.74	97.51	97.52
Extra Tree Regression	BW_1	0.52	0.04	1.92	93.07	93.11
	BW_2	0.54	0.02	1.54	98.06	98.06
XGBoost Regression	BW_1	1.16	0.05	2.22	90.73	90.79
	BW_2	1.53	0.10	3.16	91.80	91.84
K-Nearest Neighbors	BW_1	0.62	0.05	2.22	90.67	90.67
	BW_2	0.63	0.03	1.84	97.22	97.23

Table 4. Gain prediction performance

Algorithms	Gain	MAE (%)	MSE (%)	RMSE (%)	R-Square (%)	Var Score (%)
Linear Regression	G_1	37.16	46.61	68.27	25.26	25.48
	G_2	12.60	4.84	21.99	16.18	16.19
Random Forest Regression	G_1	5.77	6.05	24.59	90.30	90.31
	G_2	3.79	1.06	10.29	81.67	81.91
Decision Tree Regression	G_1	2.32	3.66	19.14	94.13	94.13
	G_2	2.08	0.75	8.65	87.05	87.15
Extra Tree Regression	G_1	2.27	3.66	19.12	94.14	94.14
	G_2	1.90	0.62	7.88	89.25	89.38
XGBoost Regression	G_1	2.83	3.72	19.28	94.04	94.04
	G_2	2.96	0.71	8.43	87.70	87.70
K-Nearest Neighbors	G_1	4.21	7.55	27.47	87.90	87.96
	G_2	2.69	1.08	10.38	81.32	81.34

It is important to emphasize that this predictive accuracy reflects the model's ability to learn the mapping between geometric parameters and gain, and does not itself contribute to or alter the gain values achieved by the antenna. The reported gain performance remains a direct outcome of the electromagnetic design process described in section 3; the ML framework instead complements this design by offering a fast, low-cost means of estimating gain for new or intermediate design configurations without recourse to repeated full-wave simulation.

5.3 Gain Validation Using K-Fold Cross-Validation

The Extra Tree gain-prediction model is evaluated with K-fold cross-validation to assess its generalization reliability without considering the physical performance of the antenna [40]. For this approach, the dataset is split into five equal subsets, each of which is used once as the testing set while the other four are used as the training set, and this process is repeated for all the folds, and the final metrics for performance are obtained by averaging the results, as shown in Figure 18. This technique provides a more robust, conservative assessment of the model's generalization than a single train-test split, helping to confirm that its predictive accuracy is not an artifact of a particular data partition. The MAE across folds ranged from 0.0072 to 0.0102 and the RMSE from 0.0145 to 0.0187, which showed a consistently low prediction error. Over folds, R^2 ranges from 0.7314 to 0.8521 (average 0.7709), somewhat lower than the single-split R^2 reported in Table 4 (94.14%). This difference is indicative of the more conservative, leave-out-fold estimate of generalization typical of k-fold validation on a modestly sized dataset (193 samples), and not any change in the antenna's actual electromagnetic performance. Cross-validation results indicate that the prediction model is reasonably stable in accuracy over data partitions. This supports the use of the prediction model as a practical, low-cost estimator for gain prediction, while the reported gain values of the antenna (Table 5) remain those obtained directly from CST simulation.

Table 5. Five-fold validation results for gain prediction

Fold(K)	MAE	MSE	RMSE	R^2
1	0.0089	0.00021	0.0145	0.8521
2	0.0072	0.00028	0.0167	0.7685
3	0.0078	0.00030	0.0173	0.7598
4	0.0085	0.00029	0.0170	0.7426
5	0.0102	0.00035	0.0187	0.7314
Average	0.0085	0.00029	0.0168	0.7709

Table 6. Comparison of the proposed 4-Port MIMO antenna with existing advanced MIMO solutions

Ref.	Antenna type	Frequency Band	Board Size	Isolation	BW (GHz)	Gain (dBi)	Efficiency (%)	ECC/DG (dB)	Machine Learning
[47]	4-Element	28GHz and 38 GHz	$3.53\lambda_0 \times 3.53\lambda_0$	> -29	5/ 4.2	10.14/ 9.5	> 91%	<0.007 / > 9.96	Yes
[50]	4-Element	28GHz	$3.19\lambda_0 \times 3.19\lambda_0$	-31.37	5.1	9.3	99%	< 0.0002, > 9.996	Yes
[51]	4-Element	28GHz	$2.24\lambda_0 \times 2.24\lambda_0$	>- 26.06	4.64	10.34	98.35%	0.0005, 9.99	Yes
[52]	2-Element	28GHz and 38 GHz	$2.28\lambda_0 \times 1.17\lambda_0$	> -30	1.03/ 1.06	7.8/6	90%	0.001/9.99	Yes
[42]	4-Element	28GHz and 38 GHz	$2.43\lambda_0 \times 2.43\lambda_0$	-33	0.6/ 0.6	7.4/ 8.1	88%/ 88.8%	< 0.005/ 9.99	No
[43]	4-Element	28GHz and 38 GHz	$1.68\lambda_0 \times 0.79\lambda_0$	> -20	0.72/ 0.5	4.15/ 7.73	80.13%/ 85.44%	< 0.03/ 9.87	No
[44]	4-Element	28GHz and 38 GHz	$1.66\lambda_0 \times 1.66\lambda_0$	> -22	0.619/ 0.56	8.5/ 8.9	90%/ 93%	3×10^{-5} / 0.99992	No
[45]	4-Element	28GHz and 38 GHz	$0.56\lambda_0 \times 1.5\lambda_0$	≥ -25	2.34/ 4.07	8/ 9.5	85%/ 90%	$\leq$ 0.0001/ 9.99	No
[46]	2-Element	28 GHz	$1.87\lambda_0 \times 1.87\lambda_0$	-19	0.85	10	-	0.002/ 9.98	Yes
Proposed	4-Element	28GHz and 38 GHz	$1.48\lambda_0 \times 1.48\lambda_0$	>-30	0.6/ 1	8.5/ 7.25	95%/ 96%	0.001/ 9.95	Yes

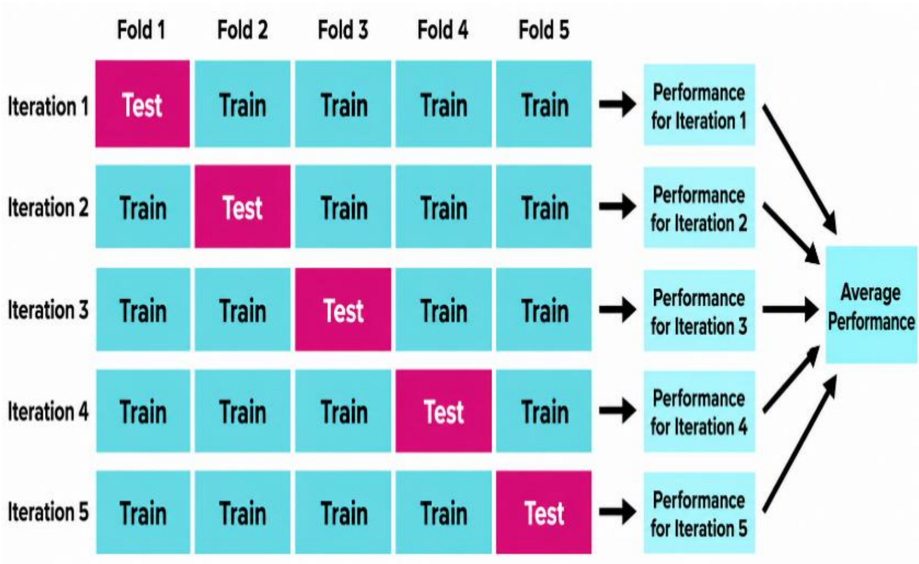

Figure 18. Actual vs. predicted 1st gain using Extra Tree regression [41].

6. COMPARISON WITH EXISTING LITERATURE

A comprehensive performance comparison is performed with recently reported mm-Wave MIMO antennas at 28 GHz and 38 GHz for 5G applications in an effort to benchmark the proposed design against the existing solutions. A detailed comparison of the proposed 4-element MIMO antenna with the existing 2-element and 4-element designs reported in the literature in terms of operational frequency bands, substrate dimensions, inter-port isolation, impedance bandwidth, radiation efficiency, ECC and DG is provided in Table 6. These parameters are affected by the electromagnetic geometry and optimization of each design.

For the bandwidth performance, the proposed design exhibits competitive dual-band operation with 0.6 GHz at 28 GHz and 1 GHz at 38 GHz, while maintaining an ultra-compact footprint of $1.48\lambda_0 \times 1.48\lambda_0$, which is significantly smaller than [47] ($3.53\lambda_0 \times 3.53\lambda_0$), [50] ($3.19\lambda_0 \times 3.19\lambda_0$), [51] ($2.24\lambda_0 \times 2.24\lambda_0$) and several other 4-element designs such as [43], [44], and [46]. The proposed slot geometry and decoupling structure achieves such compactness, which is suitable for compact mm-Wave device integration without sacrificing dual-band operation unlike the single-band designs in [50], [51]. The gain performance further validates the strength of the electromagnetic design with optimized slot geometry and parasitic decoupling structure, achieving 8.5 dBi at 28 GHz and 7.25 dBi at 38 GHz. Although the antenna peak gain is reported to be higher for the single-band designs [50] (9.3 dBi) and [51] (10.34 dBi), it does not take into account the extra design complexity of a dual-band design. The proposed antenna is competitive in terms of gain for both 28 GHz and 38 GHz bands simultaneously, compared to the dual-band 4-port designs such as [42], [43] and [45].

The most significant improvement in the proposed design is the isolation performance, which is > −30 dB port-to-port isolation in both bands, comparable or better than [50] (−31.37 dB) and [52] (>−30 dB), and much better than [43] (>−20 dB), [44] (>−22 dB), and [45] (≥−25 dB). This is done by the proposed ground and decoupling structure which presents effective mutual coupling suppression required to maintain the independent signal channels in MIMO systems.

The proposed antenna also delivers radiation efficiency of 95% at 28 GHz and 96% at 38 GHz, outperforming the dual-band designs in [42] (88%/88.8%), [43] (80.13%/85.44%), and [45] (85%/90%), and remaining competitive with the single-band efficiencies reported in [50] (99%) and [51] (98.35%), reflecting the effectiveness of the substrate and structural design choices even under the added constraint of dual-band operation.

Finally, the diversity performance of the proposed antenna remains strong, with ECC = 0.001 and DG = 9.95 dB, values that closely approach the theoretical ideal. The combination of high gain, dual-band bandwidth, ultra-low mutual coupling, excellent radiation efficiency, and compact geometry, all achieved through the proposed electromagnetic design, establishes the antenna as a robust, high-performance solution for next-generation 28/38 GHz mm-wave communication systems. Independently of this EM design contribution, the integrated ML framework provides a validated, low-cost surrogate model for predicting these performance metrics across new design configurations, reducing dependence on repeated full-wave simulation.

To evaluate this ML contribution independently of the antenna's electromagnetic performance, Table 7 compares the proposed prediction framework against recent ML-based antenna prediction studies in terms of model accuracy, computational efficiency, and prediction scope. The proposed framework achieves an R^2 of 98%, matching [9] and [11] and exceeding [47] (95.66%), [49] (92.99%), and [50] (97.83%). Only [14] (99.99%, MPR) reports higher accuracy, though MPR is limited to simpler, single-frequency relationships and does not extend to the nonlinear, multi-parameter interactions addressed here. Computationally, the framework maintains low training time and very fast inference, comparable to the tree-based models in [47]–[50] and matching the inference speed of the ANN in [11], but without its moderate training overhead, making it well suited for rapid, repeated design-iteration queries. In prediction scope, most compared works target a single output such as gain ([47], [49], [50]) or return loss/VSWR ([14]), while [48] covers both bandwidth and gain for a single band. The proposed framework predicts both bandwidth and gain across two bands (28 and 38 GHz), offering broader coverage than single-band or single-metric studies such as [48] and [9]. Regarding limitations, most models, including the proposed one, remain constrained by extrapolation beyond the training range, underscoring that prediction reliability depends on dataset diversity rather than the antenna's electromagnetic performance, which was independently validated through full-wave simulation in Section 3.

7. PRACTICAL LIMITATION IN REAL-WORLD SCENARIOS

The proposed 4-element MIMO antenna shows a promising performance and therefore can be a good candidate for future THz communication scenarios. However, a number of critical fabrication, integration and system level adaption concerns must be addressed to translate this simulated performance into real world systems as shown below:

I. The CST platform-based simulation analysis is the main focus of this effort. While these computational methods offer a useful insight into the antenna performance, they cannot fully replace physical manufacturing and measurement based experimental validation. It is important to check the practical results for 5G mm-wave systems at 28/38 GHz. This is because practical problems including measurement errors, manufacturing defects, and connector losses can significantly affect the antenna performance compared to the expected results.

II. Because the wavelengths are comparatively tiny, the construction of 28/38 GHz antennas requires excellent precision. Even minor dimensional errors or substrate irregularities can noticeably degrade important performance parameters like gain, bandwidth and impedance matching. However, the incorporation of optimization based on ML along with antennas also raises the issue of increased computational complexity and knowledge requirements, which may elevate costs and restrict application.

III. Metamaterial/Meta surface structures are not considered but they can further improve gain, bandwidth and isolation for mm-wave applications.

IV. The small size of the dataset limits the use of deep learning models, and may cause overfitting, which decreases the generalization capability. Future work with larger datasets can improve prediction accuracy and optimization of design.

Table 7. Performance comparison of the proposed and existing ML-based antenna prediction models

Ref.	ML Methods	Best ML Model	Application	Best R^2/ Accuracy	Training Time	Inference Time	Computational Complexity	Prediction parameters	Limitation
[47]	Decision Tree, XGB, Gaussian Process, Ridge	Random Forest	28 and 38 GHz band	95.66	Low	Fast	Low	Gain	Limited extrapolation capability
[48]	Decision Tree, XGB, Poisson, Lasso, Nonparametric	Lasso regression	38 GHz band	97.12	Low	Fast	Low	BW, Gain	Limited nonlinear modelling capability
[9]	Linear, Gradient Boosting, Random Forest, Extra Tree, Lasso, Decision Tree	Extra Tree	22-36 GHz	98	Low	Fast	Low	RF, BW	Limited extrapolation
[11]	Artificial Neural Network	ANN model	28 and 38 GHz	98	Moderate	Very fast	Moderate	RF, Gain	Lower accuracy for complex geometries
[49]	Decision Tree, XGB, Extra Tree, Gradient Boosting, Extra Tree	Extra Tree	28 GHz and 38 GHz	92.99	Low	Fast	Low	Gain	Higher memory consumption
[14]	Multivariate Polynomial Regression (MPR)	MPR	28 GHz	99.99	Low to Moderate	Very Fast	Moderate	BW, VSWR, Return loss	Cannot effectively model highly complex nonlinear relationships
[50]	Decision Tree, XGB, Nonparametric, Random Forest, RANSAC	Random Forest	28 GHz	97.83	Low	Fast	Low	Gain	Limited extrapolation capability
This Work	Linear, Random Forest, Decision Tree, Extra Tree, XGB, KNN	Extra Tree	28 and 38 GHz	98	Low	Very fast	Low	BW, Gain	Requires initial training dataset

8. CONCLUSION

In this paper, a compact dual-band four-port MIMO antenna is proposed for 5G mm-wave applications at 28 GHz and 38 GHz and a machine learning framework is designed for performance prediction without the need of simulation. The proposed design is based on a defected ground structure (DGS) that provides excellent inter-port isolation of more than 30 dB and gain of 8.5 dBi and 7.25 dBi with peak radiation efficiency of 96%. The four-element MIMO system had an envelope correlation coefficient below 0.001, a diversity gain over 9.95 dB and a channel capacity loss of only 0.01 bps/Hz at 28 GHz, all of which show excellent spatial diversity and spectral efficiency for dense 5G deployments. To augment this electromagnetic design and to accelerate the subsequent performance evaluation, a comprehensive ML regression framework including six algorithms was developed with key geometrical parameters as inputs. The Extra Trees Regressor provided the highest predictive accuracy among all the evaluated models, achieving R^2 values up to 98% for bandwidth and 94% for gain prediction, and K-fold cross-validation also confirmed robust generalization across unseen configurations. In the future work, the prototype antennas will be fabricated and experimentally measured for the validation of the simulated electromagnetic performance and the ML-based predictions. Furthermore, the study will extend the training dataset and investigate advanced deep learning and ensemble models to further improve the prediction accuracy and generalization, thereby enabling the faster development of next-generation mm-wave antenna systems.

REFERENCES

[1] S. Nizar Anouar B., Islem B. H., Lassaad L., and Ali G., "Millimeter-Wave Dual-Band MIMO Antennas for 5G Wireless Applications, Journal of Infrared, Millimeter, and Terahertz Waves," vol. 44, pp. 297–312, 2023. DOI: https://doi.org/10.1007/s10762-023-00914-5

[2] B. Kaur, Dadkhah S, Shoeleh F, Neto EC, Xiong P, Iqbal S, Lamontagne P, Ray S, Ghorbani AA. "Internet of things (IoT) security dataset evolution: Challenges and future directions. Internet of Things," 2023 Jul 1;22:100780.DOI:https://doi.org/10.1016/j.iot.2023.100780

[3] T. Saeidi, A. J. A. Al-Gburi, and S. Karamzadeh, "A Miniaturized Full-Ground Dual-Band MIMO Spiral Button Wearable Antenna for 5G and Sub-6 GHz Communications," Sensors, vol. 23, no. 4, p. 1997, 2023. DOI: https://doi.org/10.3390/s23041997

[4] M.M. Alam, Ouameur, M.A., M.E. Haque, Haque, M.A., Tiang, J.J., Singh, N.S.S., Alsulami, R. and S. Alzahrani, "Circular MIMO antenna with ML-based bandwidth and isolation prediction for 6G communications," Sci Rep 16, 19363 (2026). DOI: https://doi.org/10.1038/s41598-026-54274-w

[5] I.-J. Hwang Oh J.-I., Jo H.-W., Kim K.-S., Yu J.-W., Lee D.-J. "28 GHz and 38 GHz dual-band vertically stacked dipole antennas on flexible liquid crystal polymer substrates for millimeter-wave 5G cellular handsets," IEEE Trans. Antennas Propag. 2022;70(5):3223–3236. DOI: https://doi.org/10.1109/TAP.2021.3137234

[6] BA Esmail, S. Koziel "Design and optimization of metamaterial-based dual-band 28/38 GHz 5G MIMO antenna with modified ground for isolation and bandwidth improvement," IEEE Antennas and Wireless Propagation Letters. 2022 Dec 28;22(5):1069-73. DOI: https://doi.org/10.1109/LAWP.2022.3232622

[7] K Cuneray, Akcam N, Okan T, Arican GO. "28/38 GHz dual-band MIMO antenna with wideband and high gain properties for 5G applications," AEU-International Journal of Electronics and Communications. 2023 Apr 1;162:154553.DOI:https://doi.org/10.1016/j.aeue.2023.154553

[8] M. Hussain, Mousa Ali, E., Jarchavi, S.M.R., Zaidi, A., Najam, A.I., Alotaibi, A.A., Althobaiti, A. and Ghoneim, S.S., 2022. "Design and characterization of compact broadband antenna and its MIMO configuration for 28 GHz 5G applications," Electronics, 11(4), p.523. DOI: https://doi.org/10.3390/electronics11040523

[9] M. M. Alam, Yusof, N. A. T., Faudzi, A. A. M., Tomal, M. R. I., Haque, M. E., & Rahman, M. S. (2025), "Machine learning-based approach for bandwidth and frequency prediction of circular SIW antenna," Journal of King Saud University–Engineering Sciences, *37*(4), 1-19. DOI: https://doi.org/10.1007/s44444-025-00010-0

[10] MA Haque, Nirob JH, Nahin KH, Singh NS, Paul LC, Algarni AD, ElAffendi M, Ateya AA. "Regression supervised model techniques THz MIMO antenna for 6G wireless communication and IoT application with isolation prediction," Results in Engineering. 2024 Dec 1;24:103507.DOI:https://doi.org/10.1016/j.rineng.2024.103507

[11] M. M. Alam, Yusof, N. A. T., Wahab, Y. A., Karim, M. S. A., & Rahman, M. S. (2025), "Design and optimization of Π-shaped slotted dual-band SIW antenna for 5G applications," Applications of Modelling and Simulation, 9, 92-106. DOI: https://arqiipubl.com/ojs/index.php/AMS_Journal/article/view/819/213

[12] A.K. Dwivedi, N.K. Narayanaswamy, K.K.V. Penmatsa, S.K. Singh, A. Sharma, V. Singh, "Circularly polarized printed dual port MIMO antenna with polarization diversity optimized by machine learning approach for 5G NR n77/n78 frequency band applications," Sci. Rep. 13 (1) (2023) 13994. DOI: https://doi.org/10.1038/s41598-023-41302-2

[13] N. Chhaule, C. Koley, S. Mandal, A. Onen, & T. S. Ustun, "A comprehensive review on conventional and machine Learning-Assisted design of 5G microstrip patch antenna," *Electronics*, 2024, 13(19), 3819. DOI: https://doi.org/10.3390/electronics13193819

[14] M. Rana, S. M. Rabiul Islam, and S. Sarker, "Machine learning based on patch antenna design and optimization for 5 G applications at 28GHz," Results Engineering, vol. 24, p. 103366, Dec. 2024. DOI: https://doi.org/10.1016/j.rineng.2024.103366

[15] S. S. M Al-Bawri, W. M. Abdulkawi, A. A. Sheta, Md, Moniruzzaman, "A High-Performance 3D Eight-Port THz-MIMO antenna system verified with machine learning for enhanced wireless communication systems," *Int. J. Commun. Syst.* **38** (4), e6006. DOI: https://doi.org/10.1002/dac.6006

[16] S. O. Hasan, Ezzulddin, S. K., Hammd, O. S., & Mahmud, R. H. "Design and performance analysis of rectangular microstrip patch antennas using different feeding techniques for 5G applications," International journal of electrical and computer engineering systems, 14(8), 2023, 833-841. DOI: https://doi.org/10.32985/ijeces.14.8.2

[17] M.M. Alam, Ouameur M.A., Hasan M.M., Alyami G., Haque M.A., Alshammari M.A., Singh N.S., Shaman H. "Machine learning-based dual-band circular MIMO antennas for high-performance 6G IoT system," Results Engineering, 2025:108107. DOI: https://doi.org/10.1016/j.rineng.2025.108107

[18] Al-Atyar, R. A., Farahat, A. E., Hussein, K. F. A., Shaalan, A. A., & M. F. Ahmed, "Dual-Band (28/38 GHz)–Loaded Patch Antenna for Millimeter-Wave Communication," Journal of Infrared, Millimeter, and Terahertz Waves, 46(3), 22, 2025. DOI: https://doi.org/10.1007/s10762-025-01036-w

[19] Y.-F. Liu, L.-Y. Xiao, and Q. H. Liu, "Machine learning-based design scheme for multifunctional antenna arrays with reconfigurable scattering patterns," IEEE Trans. Antennas Propag., vol. 73, no. 7, pp. 4535–4548, Jul. 2025. DOI: https://doi.org/10.1109/TAP.2025.3552213

[20] F. Taher, Hamadi, H.A., Alzaidi, M.S., Alhumyani, H., Elkamchouchi, D.H., Elkamshoushy, Y.H., Haweel, M.T.,

Sree, M.F.A. and Fatah, S.Y.A., "Design and analysis of circular polarized two-port MIMO antennas with various antenna element orientations," Micromachines, 14(2), p.380, 2023. DOI: https://doi.org/10.3390/mi14020380

[21] S.-H. Kim, J.-Y. Chung, "Analysis of the envelope correlation coefficient of MIMO antennas connected with suspended lines," J. Electromagn. Eng. Sci 20 (2), 83–90, Apr.2020.DOI: https://doi.org/10.26866/JEES.2020.20.2.83

[22] H. Wang, Q. Zheng, Q. Li and X. -X. Yang, "Isolation Improvement and Bandwidth Enhancement of Dual-Band MIMO Antenna Based on Metamaterial Wall," in IEEE Antennas and Wireless Propagation Letters, vol. 24, no. 5, pp. 1144-1148, May 2025. DOI: https://doi.org/10.1109/LAWP.2025.3527688

[23] M.M. Basha, P. Pradeep, S. Gundala, J. Syed, "Design of compact and high gain dual-band four-port MIMO antenna array for mm-wave 5G communications," Results Eng. 25 (2025) 104153. DOI: https://doi.org/10.1016/j.rineng.2025.104153

[24] Y. Amraoui, I. Halkhams, R.E. Alami, M.O. Jamil, H. Qjidaa, "High gain MIMO antenna with multiband characterization for terahertz applications," Sci. Afr. 26 (2024) e02380. DOI: https://doi.org/10.1016/j.sciaf.2024.e02380

[25] X. Yang, "Circularly polarized antenna array synthesis based on machine-learning-assisted surrogate modeling," IEEE Trans. Antennas Propag., vol. 72, no. 2, pp. 1469–1482, Feb. 2024. DOI: https://doi.org/10.1109/TAP.2023.3335808

[26] S. Xi, J. Cai, L. Shen, Q. Li, and G. Liu, "Dual-Band MIMO Antenna with Enhanced Isolation for 5G NR Application," Micromachines, vol. 14, no. 1, p. 95, Dec. 2022. DOI: https://doi.org/10.3390/mi14010095

[27] Y. Zhong, P. Renner, W. Dou, G. Ye, J. Zhu, and Q. H. Liu, "A machine learning generative method for automating antenna design and optimization," IEEE J. Multiscale Multiphys. Comput. Tech., vol. 7, pp. 285–295, 2022. https://doi.org/10.1109/JMMCT.2022.3211178

[28] M. Bilal, S. I. Naqvi, N. Hussain, Y. Amin, and N. Kim, "High-Isolation MIMO Antenna for 5G Millimeter-Wave Communication Systems," *Electronics*, vol. 11, no. 6, p. 962, Mar. 2022. DOI: https://doi.org/10.3390/electronics11060962

[29] M.M. Alam, Rahman, M.S., Karim, M.S.A., Wahab, Y.A. and Yusof, N.A.T., "Design and optimization of a high-efficiency circular SIW patch antenna for satellite communication," Digital Communications and Networks, Volume 12, Issue 6, June 2026, Pages 977-993. DOI: https://doi.org/10.1016/j.dcan.2026.03.001

[30] J Chen, de Hoogh K, Gulliver J, Hoffmann B, Hertel O, Ketzel M, Bauwelinck M, Van Donkelaar A, Hvidtfeldt UA, Katsouyanni K, Janssen NA. "A comparison of linear regression, regularization, and machine learning algorithms to develop Europe-wide spatial models of fine particles and nitrogen dioxide," Environment international. 2019 Sep 1;130:104934. DOI: https://doi.org/10.1016/j.envint.2019.104934

[31] X. Zhu, X. Hu, L. Yang, W. Pedrycz and Z. Li, "A Development of Fuzzy-Rule-Based Regression Models Through Using Decision Trees, " in IEEE Transactions on Fuzzy Systems, vol. 32, no. 5, pp. 2976-2986, May 2024. DOI: https://doi.org/10.1109/TFUZZ.2024.3365572

[32] D. Borup, Christensen, B. J., Mühlbach, N. S., & Nielsen, M. S. (2023). "Targeting predictors in random forest regression," International Journal of Forecasting, *39*(2), 841-868. DOI: https://doi.org/10.1016/j.ijforecast.2022.02.010

[33] S.R. Shakya, M. Kube, Z. Zhou, "A comparative analysis of machine learning approach for optimizing antenna design," Int. J. Microw. Wirel. Technol. (Aug. 2023) 1–11. DOI: https://doi.org/10.1017/S1759078723001009

[34] AI Osman, Ahmed AN, Chow MF, Huang YF, El-Shafie A. "Extreme gradient boosting (Xgboost) model to predict the groundwater levels in Selangor Malaysia. Ain Shams Engineering Journal," 2021 Jun 1;12(2):1545-56. DOI: https://doi.org/10.1016/j.asej.2020.11.011

[35] S. Koziel, Pietrenko-Dabrowska, A. & L. Leifsson, "Antenna optimization using machine learning with reduced-dimensionality surrogates," Sci. Rep. 14(1), 21567. DOI: https://doi.org/10.1038/s41598-024-72478-w

[36] S. M. Robeson and C. J. Willmott, "Decomposition of the mean absolute error (MAE) into systematic and unsystematic components," *PLOS ONE*, vol. 18, no. 2, p. e0279774, Feb. 2023. DOI: https://doi.org/10.1371/journal.pone.0279774

[37] MM Alam, Tomal MR, Faudzi AA, Yusof NA, "ANN-Enabled Gain Prediction and Optimization in Dual-Band SIW Antenna Designs for 5G Networks. Journal of Telecommunications and Information Technology," 2026 Mar 2:69-78. DOI: https://doi.org/10.26636/jtit.2026.1.2424

[38] P. Takyi-Aninakwa, S. Wang, H. Zhang, Y. Xiao, C. Fernandez, "A NARX network optimized with an adaptive weighted square-root cubature Kalman filter for the dynamic state of charge estimation of lithium-ion batteries," J. Energy Storage 68 (2023) 107728. DOI: https://doi.org/10.1016/j.est.2023.107728

[39] Gelman A, Goodrich B, Gabry J, Vehtari A. "R-squared for Bayesian regression models," The American Statistician, 2019 Jul 3. DOI: https://doi.org/10.1080/00031305.2018.1549100

[40] G. Jiang, and W. Wang, "Error estimation based on variance analysis of k-fold cross-validation," Pattern Recognition, 69, pp.94-106, 2021. DOI: https://doi.org/10.1016/j.patcog.2017.03.025

[41] T. Fushiki, "Estimation of prediction error by using *K*-fold cross-validation," Stat Comput **21**, 137–146 (2021). DOI: https://doi.org/10.1007/s11222-009-9153-8

[42] R.R. Elsharkawy, Hussein, K.A. & Farahat, A.E. "Dual-Band (28/38 GHz) Compact MIMO Antenna System for Millimeter-Wave Applications," J Infrared Milli Terahz Waves 44, 1016–1037 (2023). DOI: https://doi.org/10.1007/s10762-023-00943-0

[43] R.N. Tiwari, Sharma, D., Singh, P. *et al.* "A flexible dual-band 4 × 4 MIMO antenna for 5G mm-wave 28/38 GHz wearable applications," Sci Rep 14, 14324 (2024). DOI: https://doi.org/10.1038/s41598-024-65023-2

[44] R.H. Elabd, Al-Gburi, A.J.A. "Super-Compact 28/38 GHz 4-Port MIMO Antenna Using Metamaterial-Inspired EBG Structure with SAR Analysis for 5G Cellular Devices," J Infrared Milli Terahz Waves 45, 35–65 (2024). DOI: https://doi.org/10.1007/s10762-023-00959-6

[45] S. Chidurala, Amara, P.R. "Design and Analysis of Compact Dual Band 4-Port MIMO Antenna for 5G 28/38 GHz Millimeter-Wave Communication," J Infrared Milli Terahz Waves 46, 60 (2025). DOI: https://doi.org/10.1007/s10762-025-01076-2

[46] J.K. Rai, Ranjan, P., Kumar, S., Chowdhury, R., Kumar, S. and Sharma, A., 2024. "Machine learning-enabled two-port wideband MIMO hybrid rectangular dielectric resonator antenna for n261 5G NR millimeter wave," International Journal of Communication Systems, *37*(16), p.e5898. DOI: https://doi.org/10.1002/dac.5898

[47] M.A. Haque, Ananta, R.A., Ahammed, M.S. et al. "High-isolation dual-band MIMO antenna for next-generation 5G wireless networks at 28/38 GHz with machine learning-based gain prediction," Sci Rep 15, 20782 (2025). DOI: https://doi.org/10.1038/s41598-025-02646-z

[48] MA Haque, Ahammed MS, Socheatra S, Ananta RA, Nirob MJ, Singh NS, Jizat NM, Alsowail S, Al-Bawri SS. "Machine learning based compact MIMO antenna array for 38 GHz millimeter wave application with robust isolation and high efficiency performance," Results in Engineering.

2025 Mar 1;25:104006. DOI: https://doi.org/10.1016/j.rineng.2025.104006

[49] R.A. Ananta, Alyami, G. et al., "Regression machine learning-based highly efficient dual band MIMO antenna design for mm-Wave 5G application and gain prediction," Sci Rep 15, 28730 (2025). DOI: https://doi.org/10.1038/s41598-025-13514-1

[50] M.A. Haque, Nirob, J.H., Nahin, K.H. et al., "Machine learning-based technique for gain prediction of mm-wave miniaturized 5G MIMO slotted antenna array with high isolation characteristics," Sci Rep 15, 276 (2025). DOI: https://doi.org/10.1038/s41598-024-84182-w

[51] Haque MA, Ahammed MS, Ananta RA, Aljaloud K, Jizat NM, Abdulkawi WM, Nahin KH, Al-Bawri SS. "Broadband high gain performance MIMO antenna array for 5 G mm-wave applications-based gain prediction using machine learning approach," Alexandria Engineering Journal. 2024 Oct 1;104:665-79. DOI: https://doi.org/10.1016/j.aej.2024.08.025

[52] D. Khan, Ahmad, A. & Choi, DY. ,"Dual-band 5G MIMO antenna with enhanced coupling reduction using metamaterials," Sci Rep 14, 96 (2024). DOI: https://doi.org/10.1038/s41598-023-50446-0